Supporting Information for

Pyrene Containing Conjugated Organic Microporous Polymers for Photocatalytic Hydrogen Evolution from Water

Mohamed Gamal Mohamed,[a,b#] Mohamed Hammad Elsayed,[c,d#] Ahmed M. Elewa,[c] Ahmed F. M. EL-Mahdy,[a] Cheng-Han Yang,[a] Ahmed A.K. Mohammed,[b] Ho-Hsiu Chou,[c*] and Shiao-Wei Kuo[a,e*]

[a]Department of Materials and Optoelectronic Science, Center of Crystal Research, National Sun Yat-Sen University, Kaohsiung 804, Taiwan.

[b]Chemistry Department, Faculty of Science, Assiut University, Assiut, 71516, Egypt.

[c]Department of Chemical Engineering, National Tsing Hua University, Hsinchu 30013, Taiwan.

[d]Department of Chemistry, Faculty of Science, Al-Azhar University, Nasr City 11884, Cairo, Egypt.

[e]Department of Medicinal and Applied Chemistry, Kaohsiung Medical University, Kaohsiung 807, Taiwan.

[#] These authors contributed equally.

*To whom correspondence should be addressed

E-mail: **kuosw@faculty.nsysu.edu.tw**, and **hhchou@mx.nthu.edu.tw**

Characterization

FTIR spectra were recorded using a Bruker Tensor 27 FTIR spectrophotometer and the conventional KBr disk method; 32 scans were collected at a spectral resolution of 4 cm^{-1}; the films used in this study were sufficiently thin to obey the Beer–Lambert law. DSC analyses were performed using a TA Q-20 DSC apparatus; all samples were placed in hermetic Al pans with lids and heated from 40 to 350 °C at a heating rate of 20 °C min^{-1} under a N_2 flow rate of 50 mL min^{-1}. Wide-angle X-ray diffraction (WAXD) patterns were recorded using the wiggler beamline BL17A1 of the National Synchrotron Radiation Research Center (NSRRC), Taiwan; a triangular bent Si (111) single crystal was used to obtain a monochromated beam having a wavelength (λ) of 1.33 Å. A triangular bent Si (111) single crystal was used to obtain a monochromated beam having a wavelength (λ) of 1.33 Å. Cross-polarization with MAS (CP/MAS) was used to acquire ^{13}C NMR spectral data at 75.5 MHz. The CP contact time was 2 ms; $_{1}H$ decoupling was applied during data acquisition. The decoupling frequency corresponded to 32 kHz. The MAS sample spinning rate was 10 kHz. TEM images were recorded using a JEOL JEM-2010 instrument operated at 200 kV. FE-SEM was conducted using a JEOL JSM7610F scanning electron microscope; samples were subjected to Pt sputtering for 100 s prior to observation. BET surface area and porosimetry measurements of the prepared samples (ca. 40–100 mg) were performed using BEL Master™ and BEL sim™ (v. 3.0.0). Nitrogen isotherms were generated through incremental exposure to ultrahigh-purity N_2 (up to ca. 1 atm) in a liquid N_2 bath (77 K). Surface parameters were determined using BET adsorption models in the instrument's software. TGA was performed using a TA Q-50 analyzer under a flow of N_2; the samples were sealed in a Pt cell and heated from 40 to 800 °C at a heating rate of 20 °C min^{-1} under a N_2 flow of 60 mL min^{-1}. UV–Vis spectra were recorded at 25 °C using a Jasco V-570 spectrometer, with EtOH as the solvent.

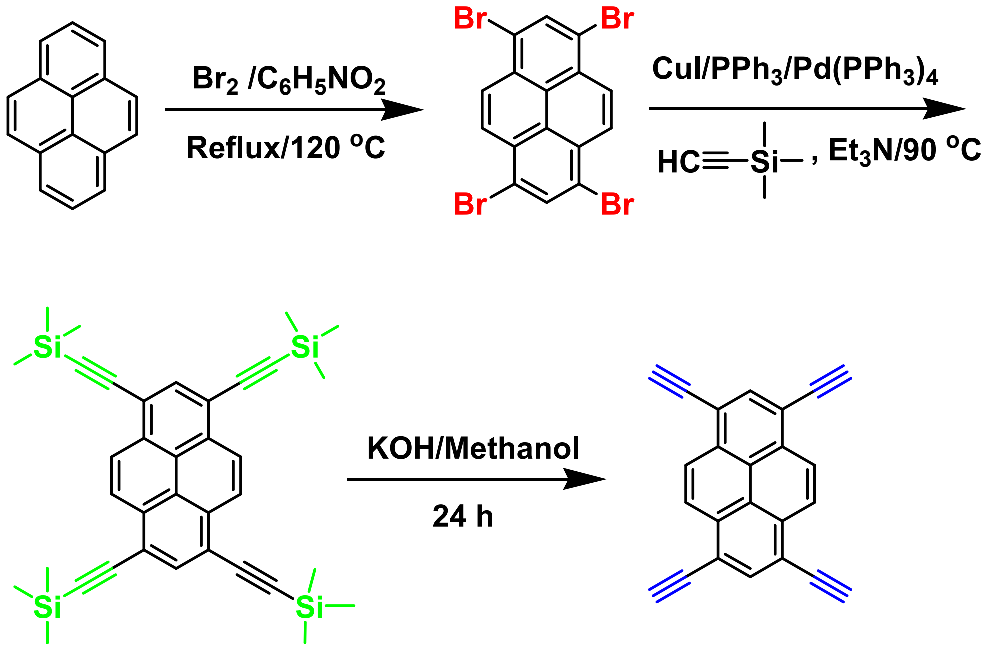

Scheme S1. Synthesis of Py-Br_4, Py-TMS and Py-T.

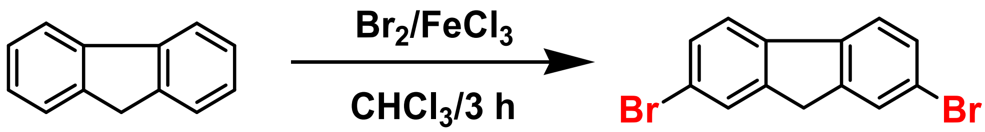

Scheme S2. Synthesis of F-Br_2.

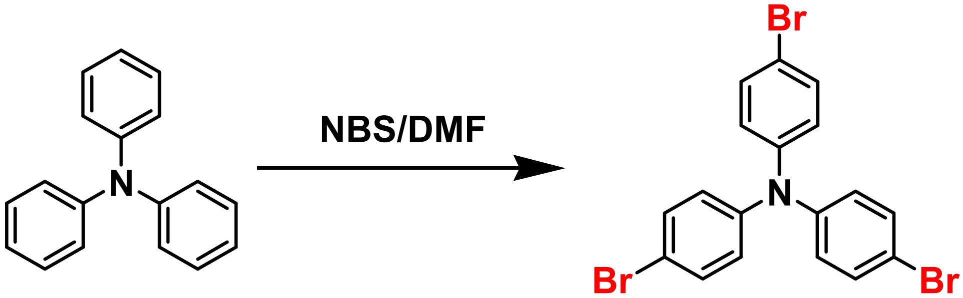

Scheme S3. Synthesis of TPA-Br_3.

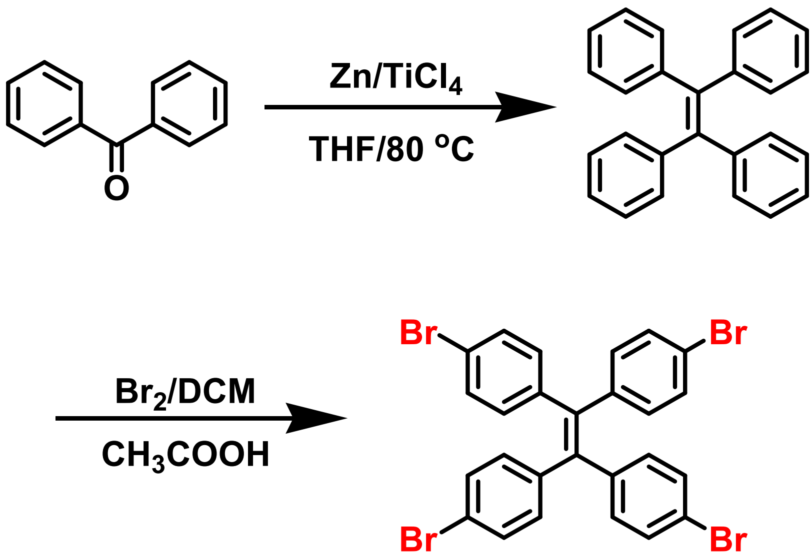

Scheme S4. Synthesis of TPE and TPE-Br_4.

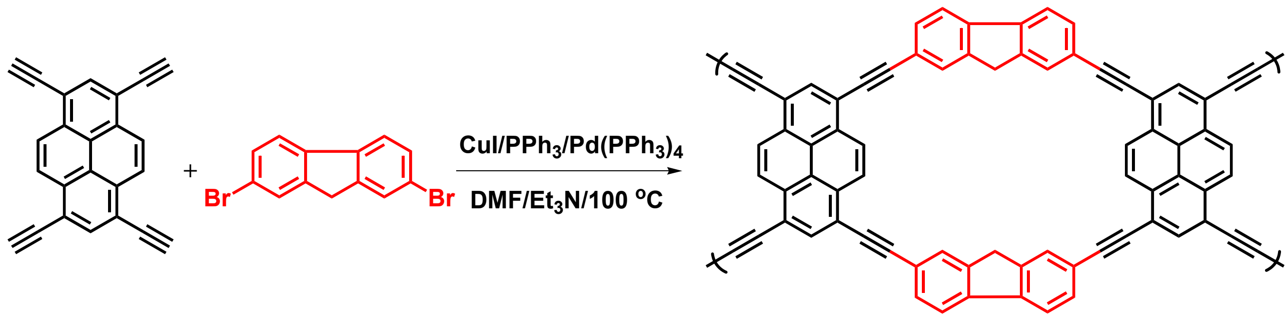

Scheme S5. Synthesis of Py-F-CMP.

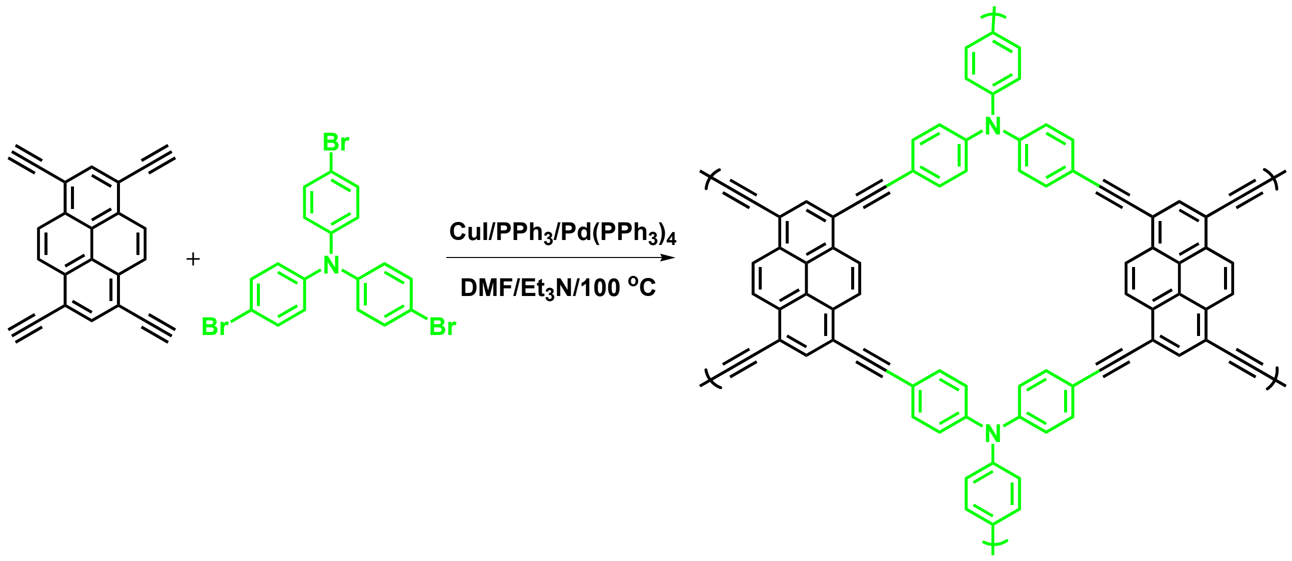

Scheme S6. Synthesis of Py-TPA-CMP.

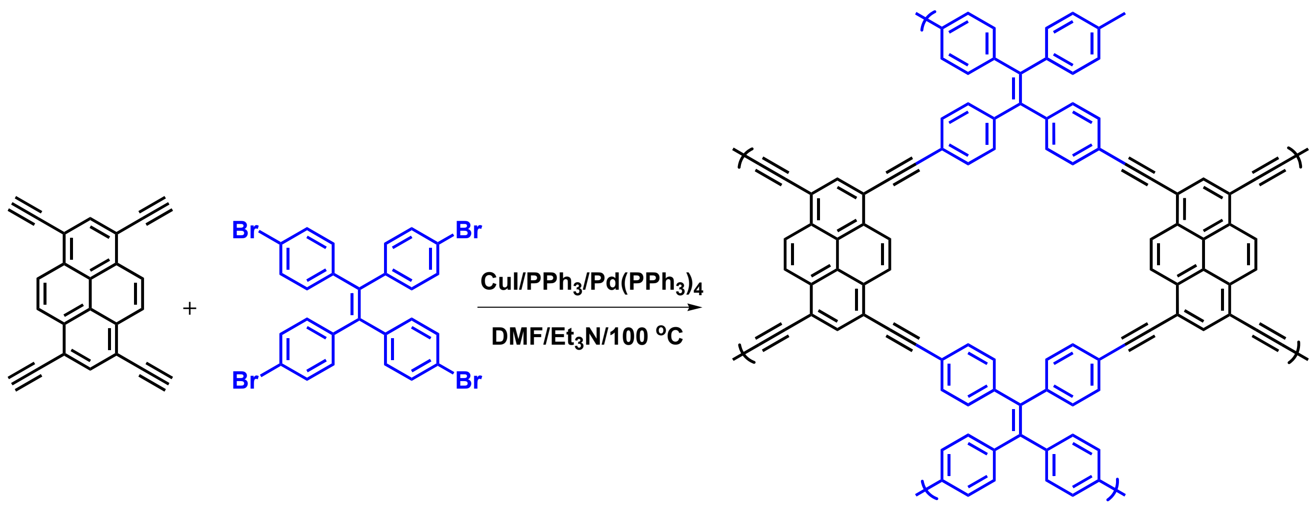

Scheme S7. Synthesis of Py-TPE-CMP.

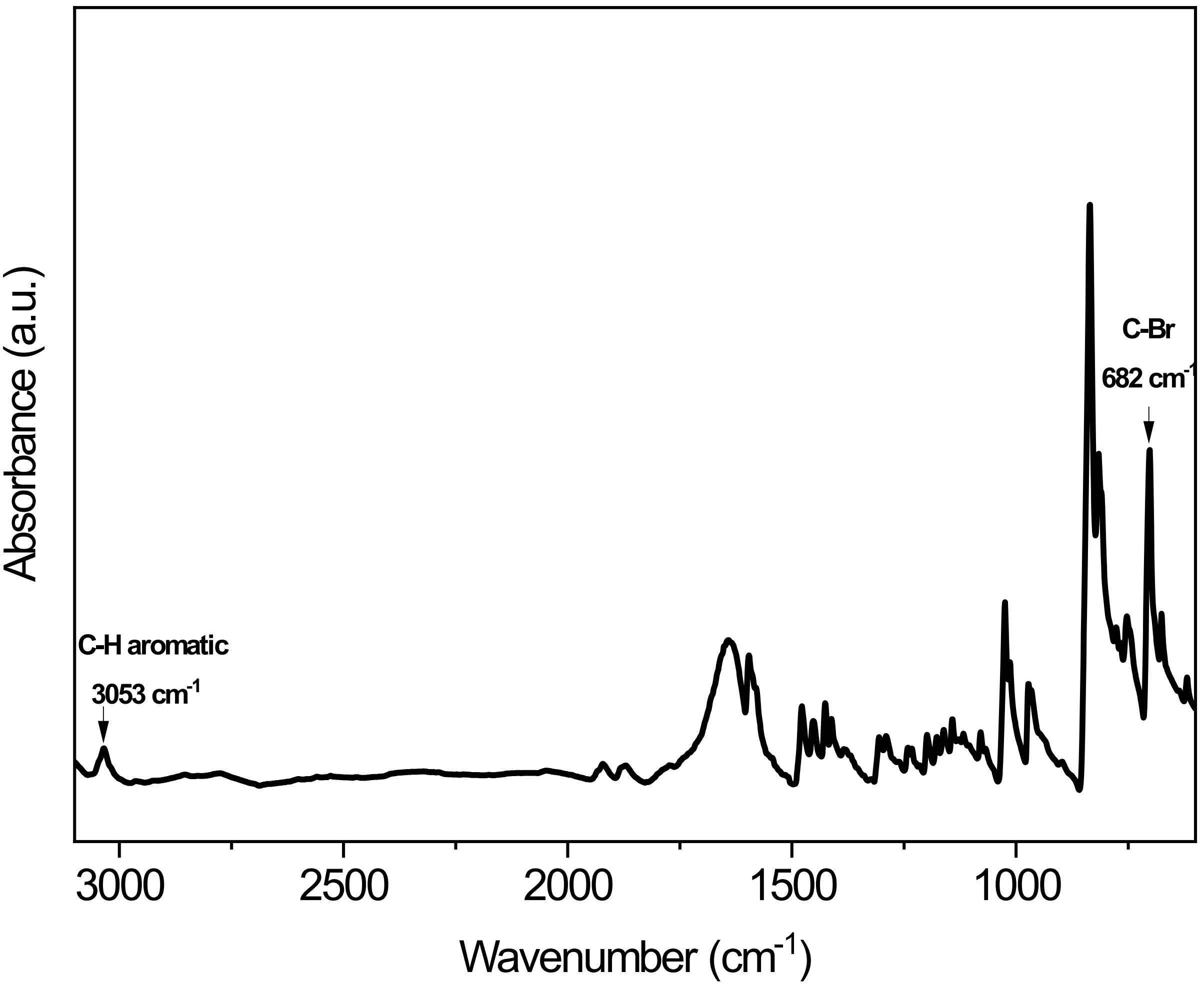

Figure S1. FT-IR spectrum of Py-Br_4.

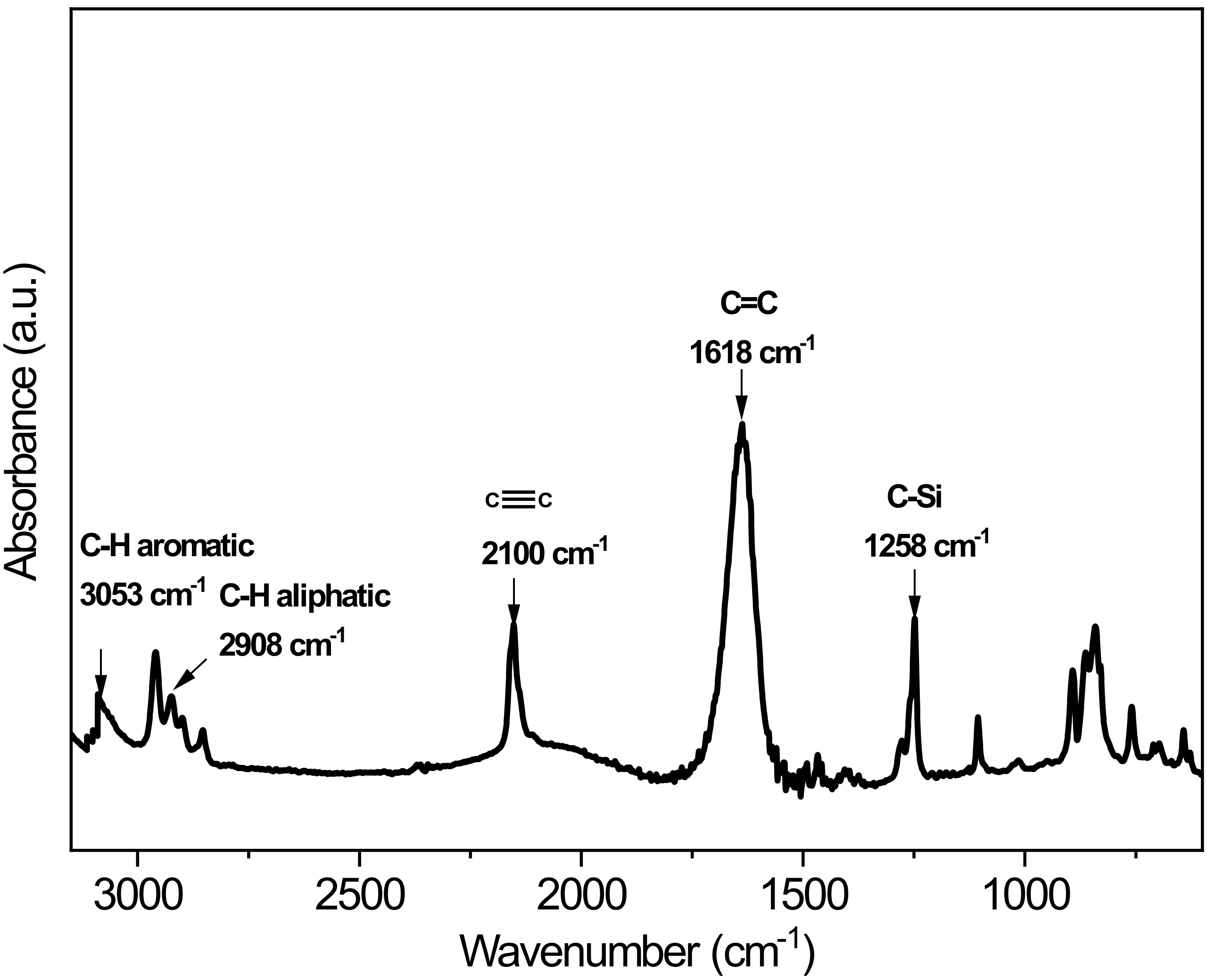

Figure S2. FT-IR spectrum of Py-TMS.

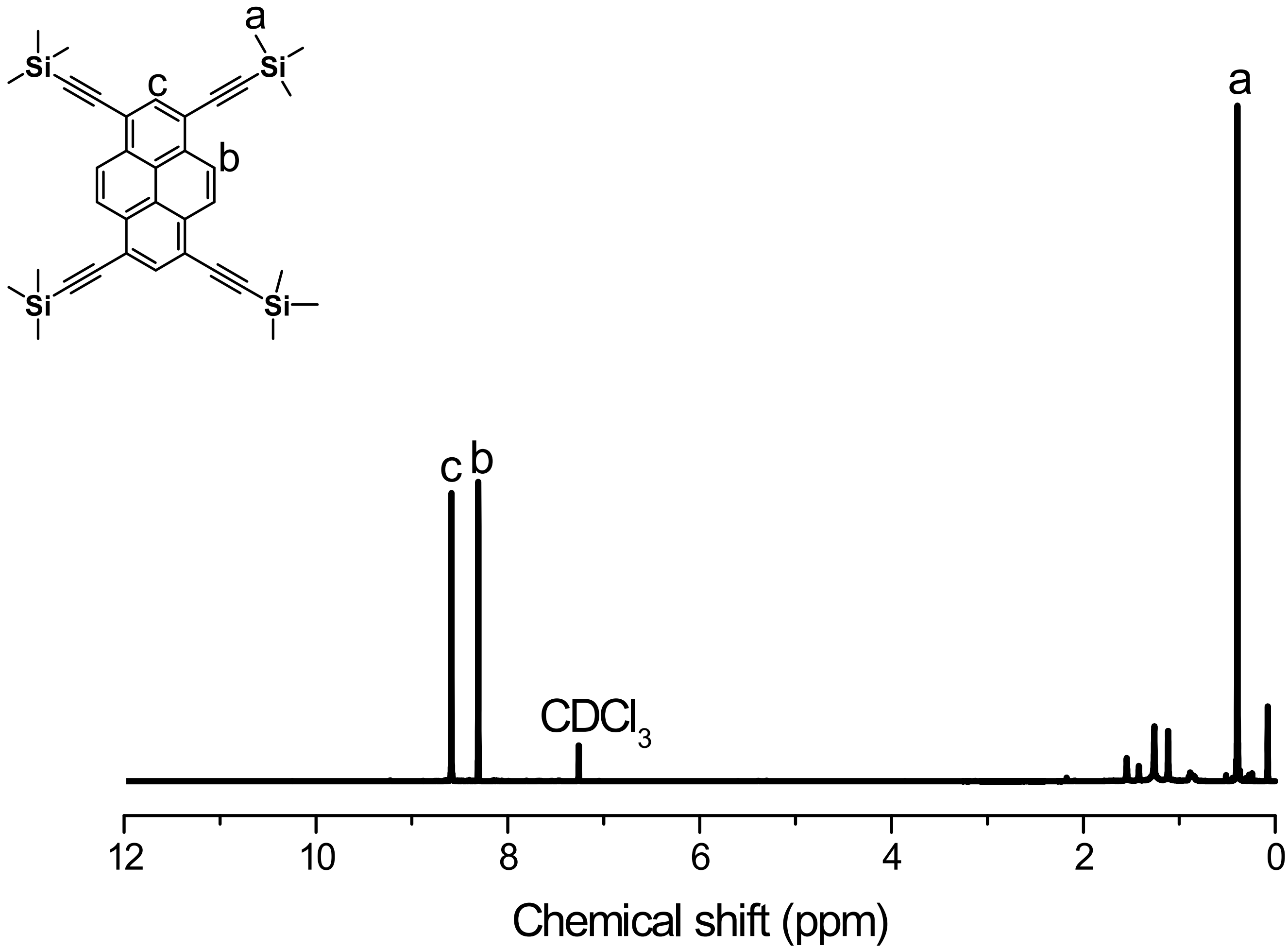

Figure S3. ^{1}H NMR spectrum of Py-TMS.

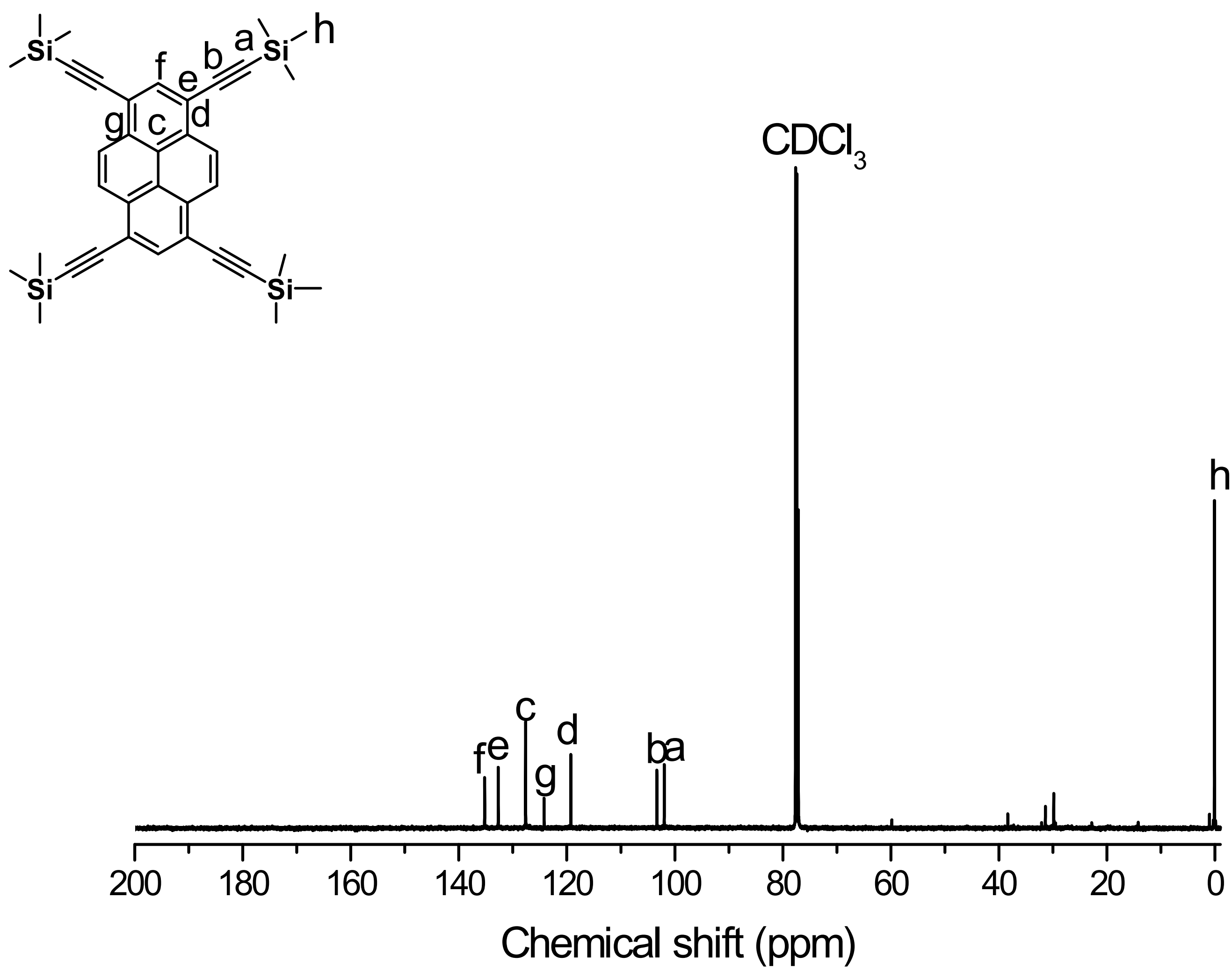

Figure S4. ^{13}C NMR spectrum of Py-TMS.

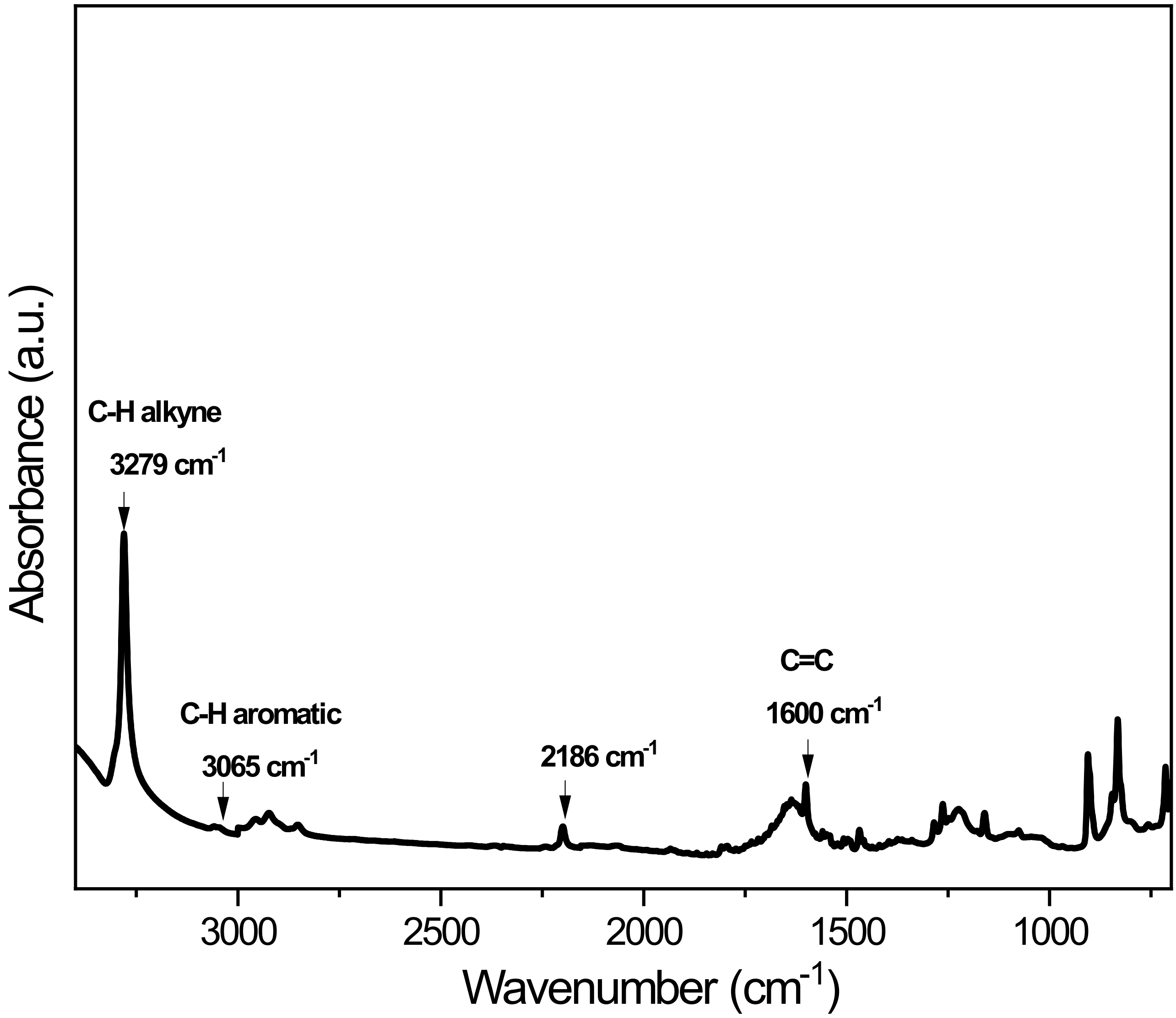

Figure S5. FT-IR spectrum of Py-T.

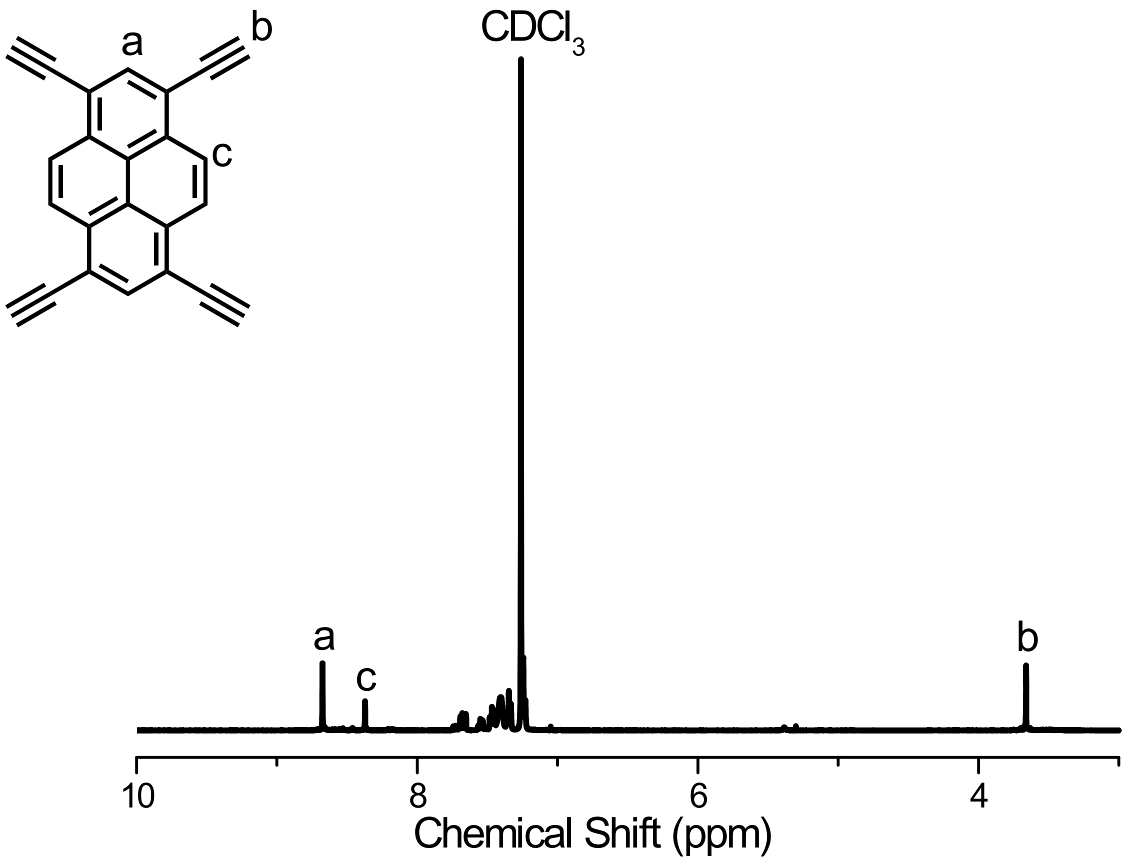

Figure S6. ^{1}H NMR spectrum of Py-T.

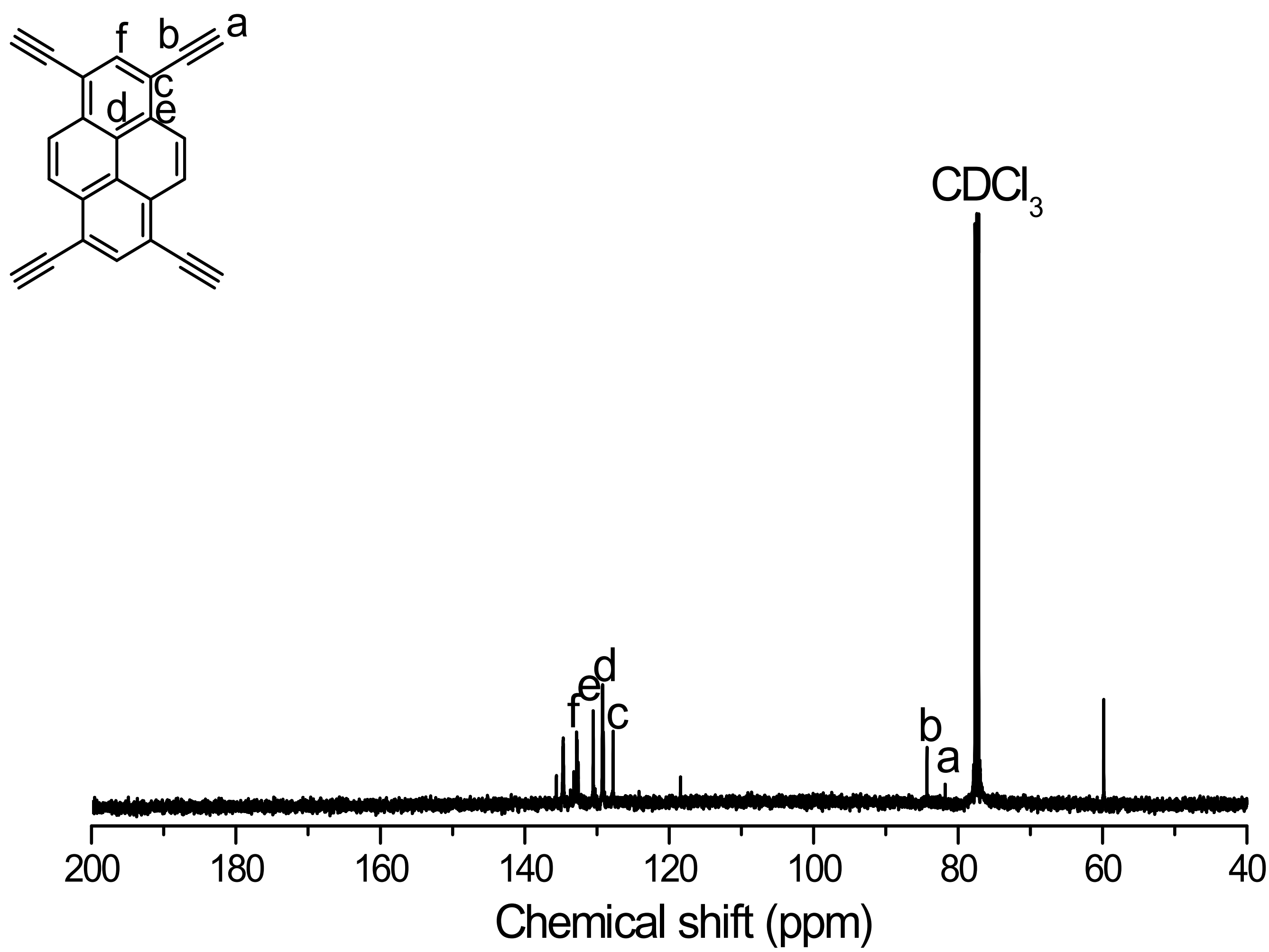

Figure S7. ^{13}C NMR spectrum of Py-T.

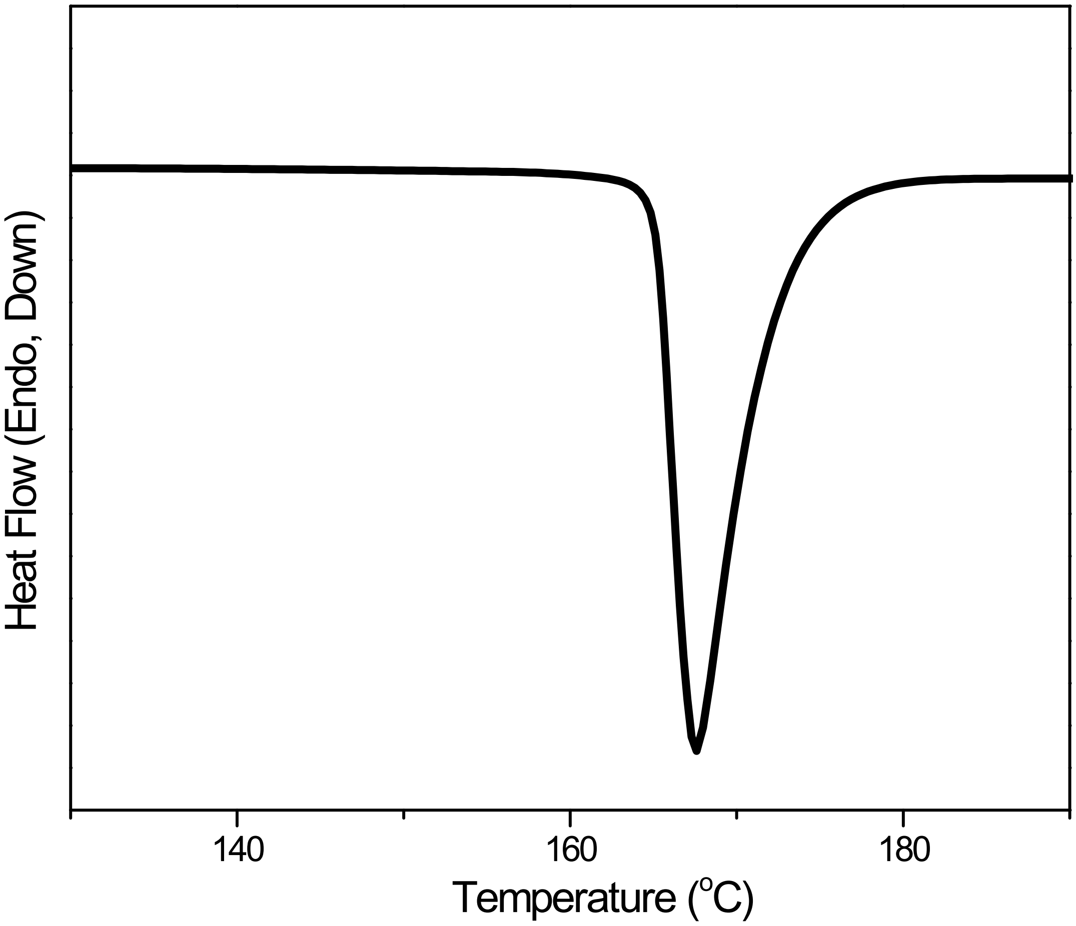

Figure S8. DSC profile of F-Br_2.

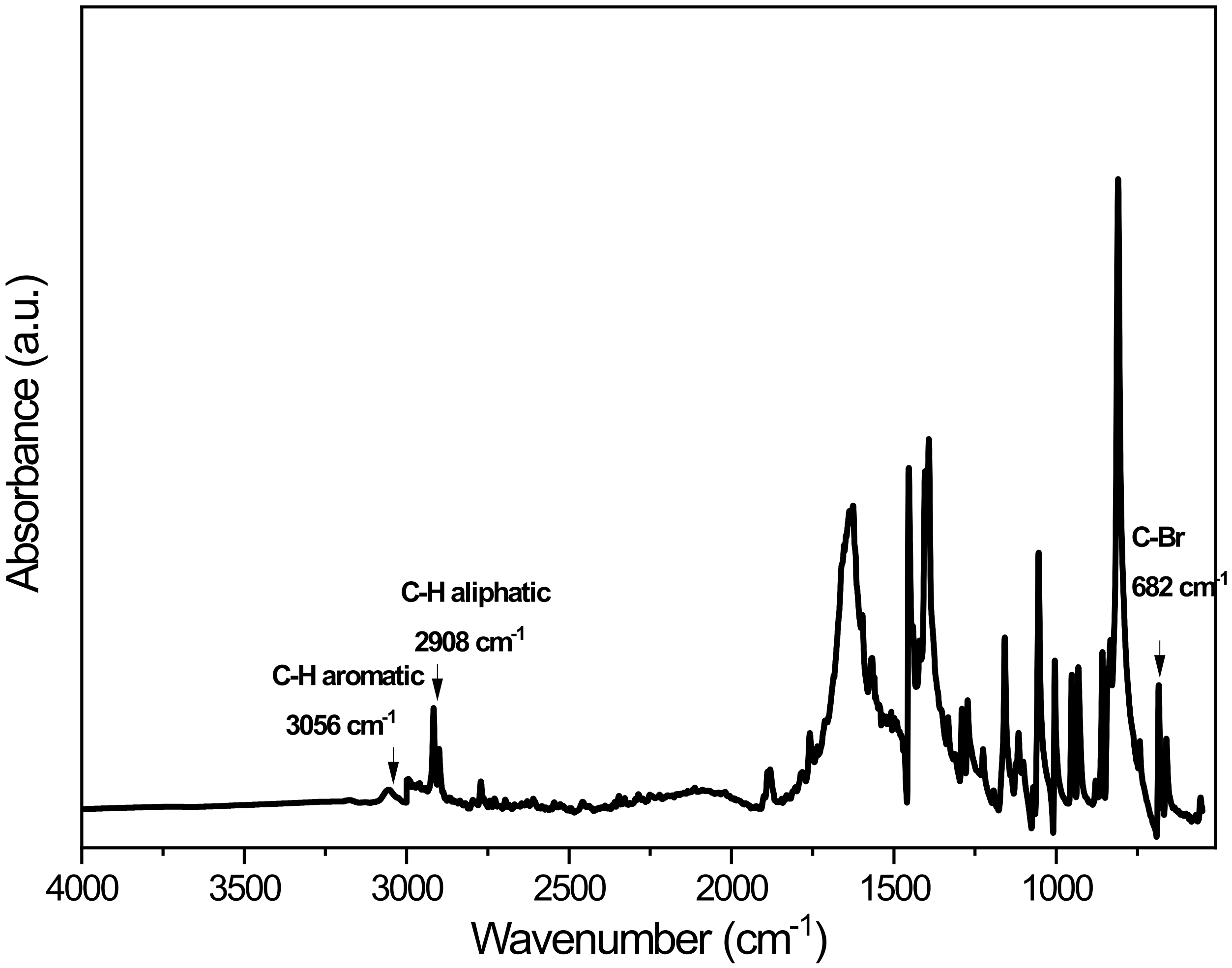

Figure S9. FT-IR spectrum of F-Br_2.

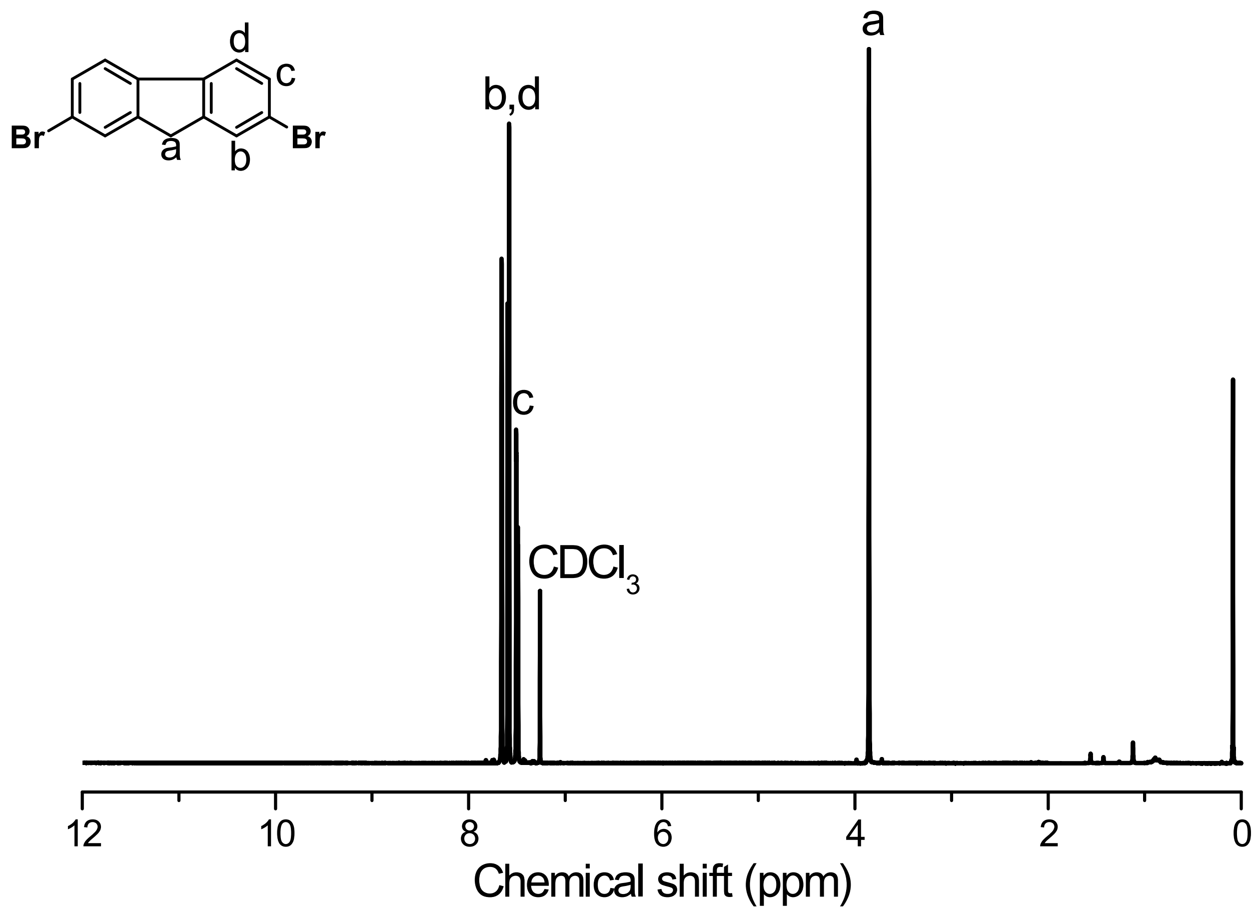

Figure S10. ^{1}H NMR spectrum of F-Br$_2$.

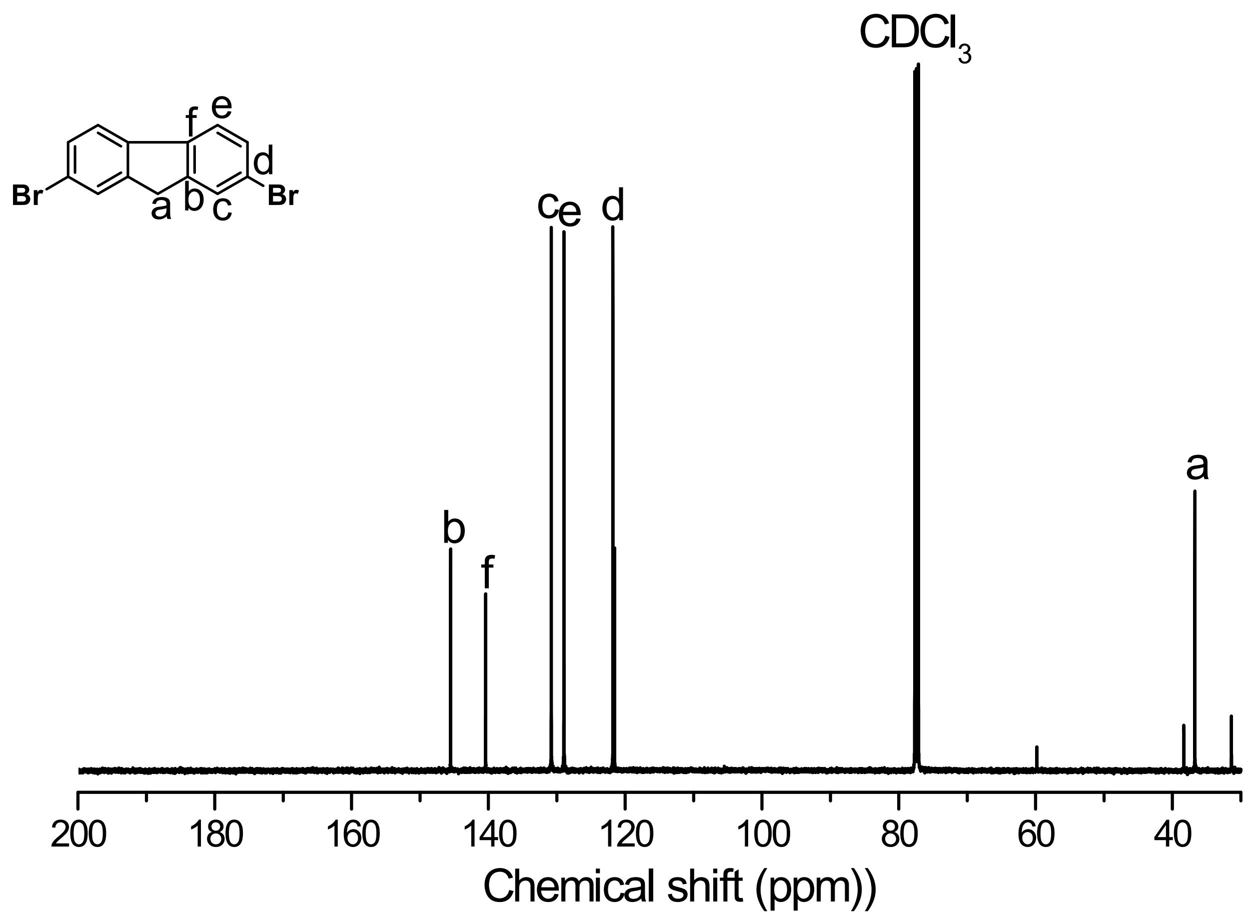

Figure S11. ^{13}C NMR spectrum of F-Br_2.

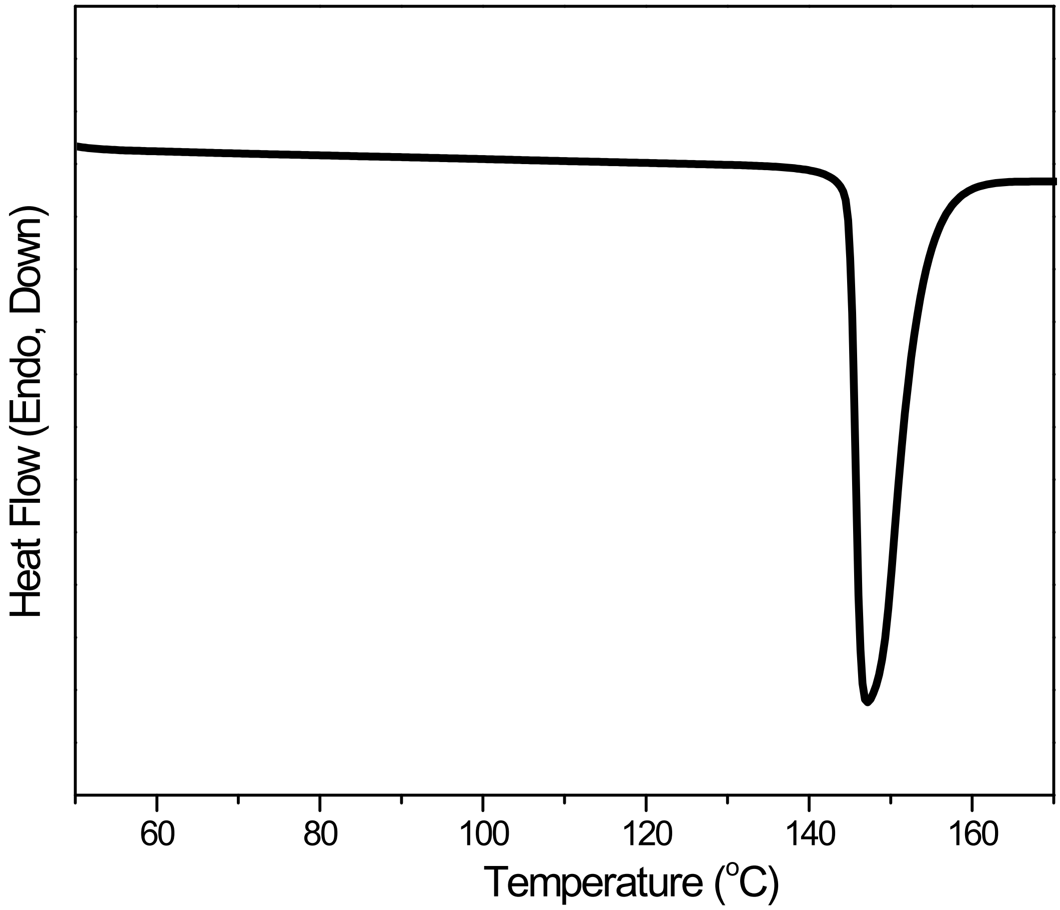

Figure S12. DSC profile of TPA-Br_3.

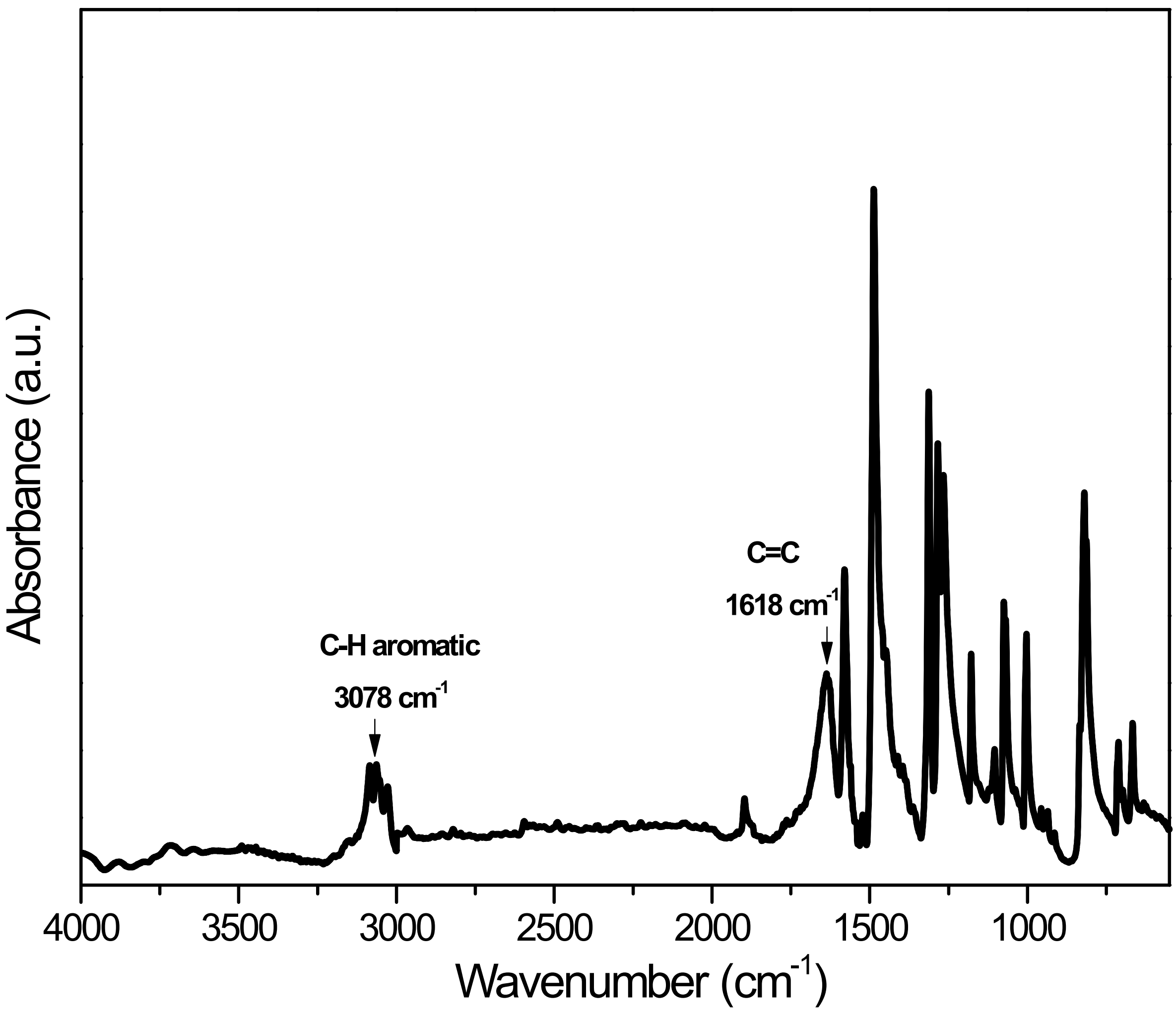

Figure S13. FT-IR spectrum of TPA-Br_3.

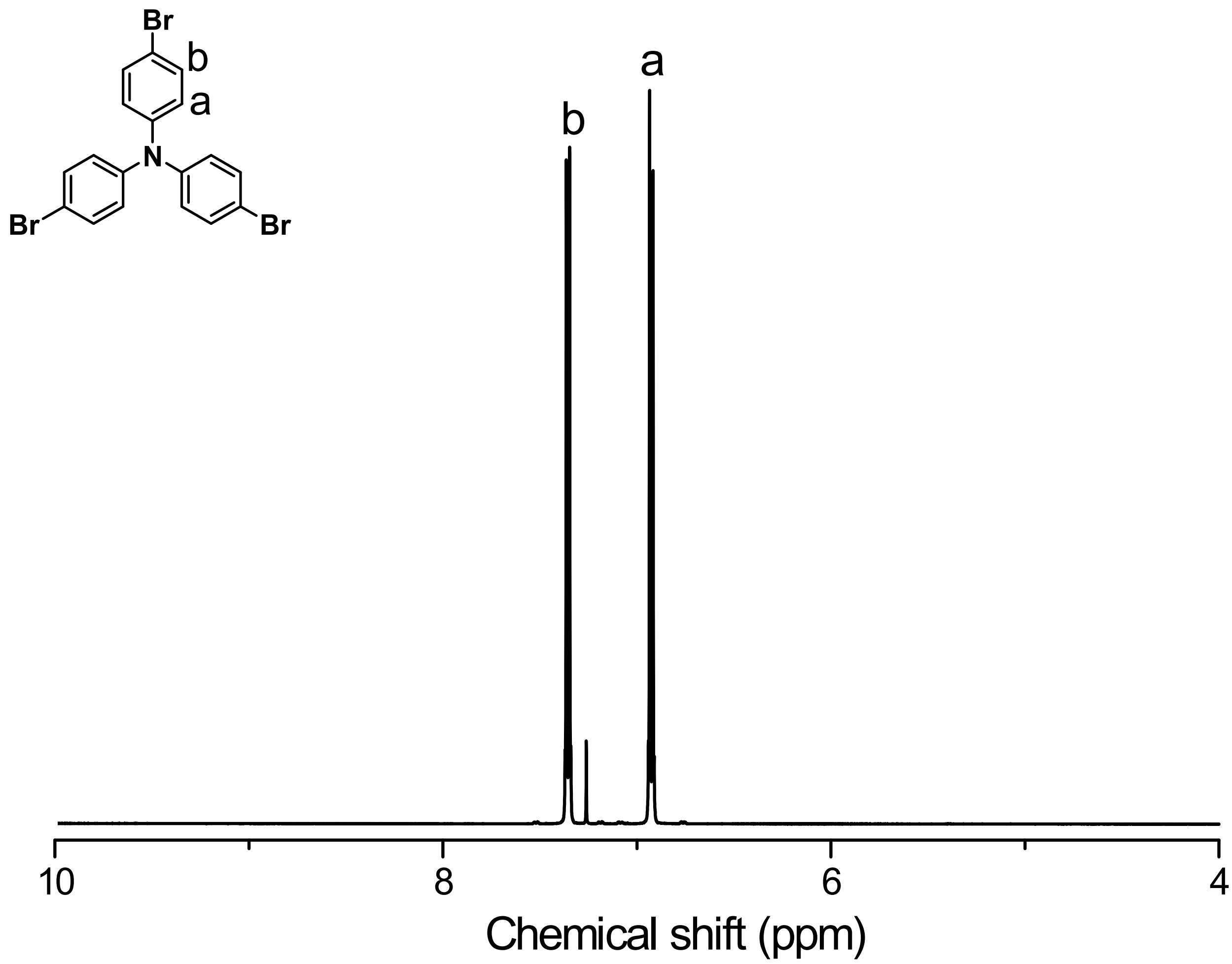

Figure S14. ^{1}H NMR spectrum of TPA-Br_3.

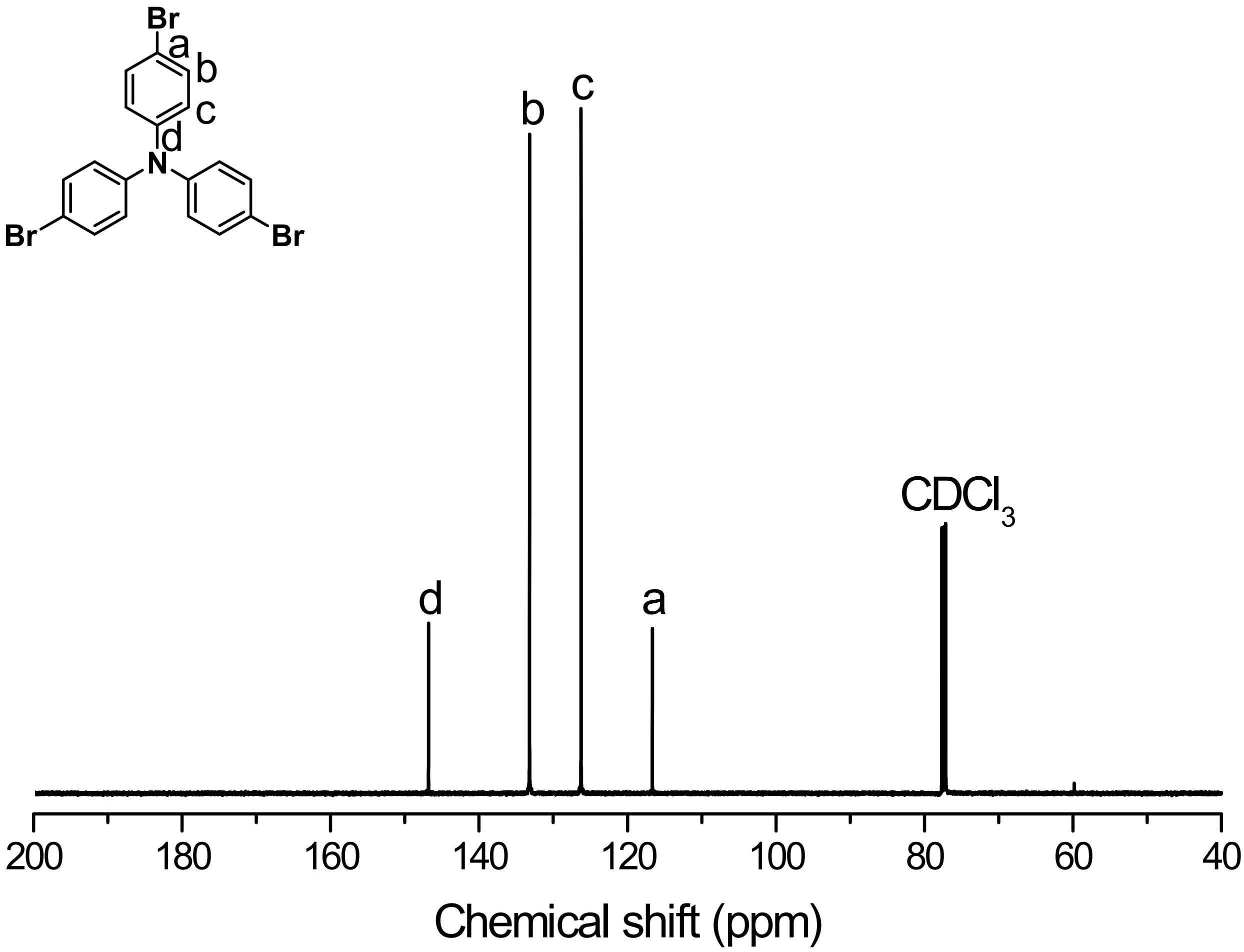

Figure S15. ^{13}C NMR spectrum of TPA-Br_3.

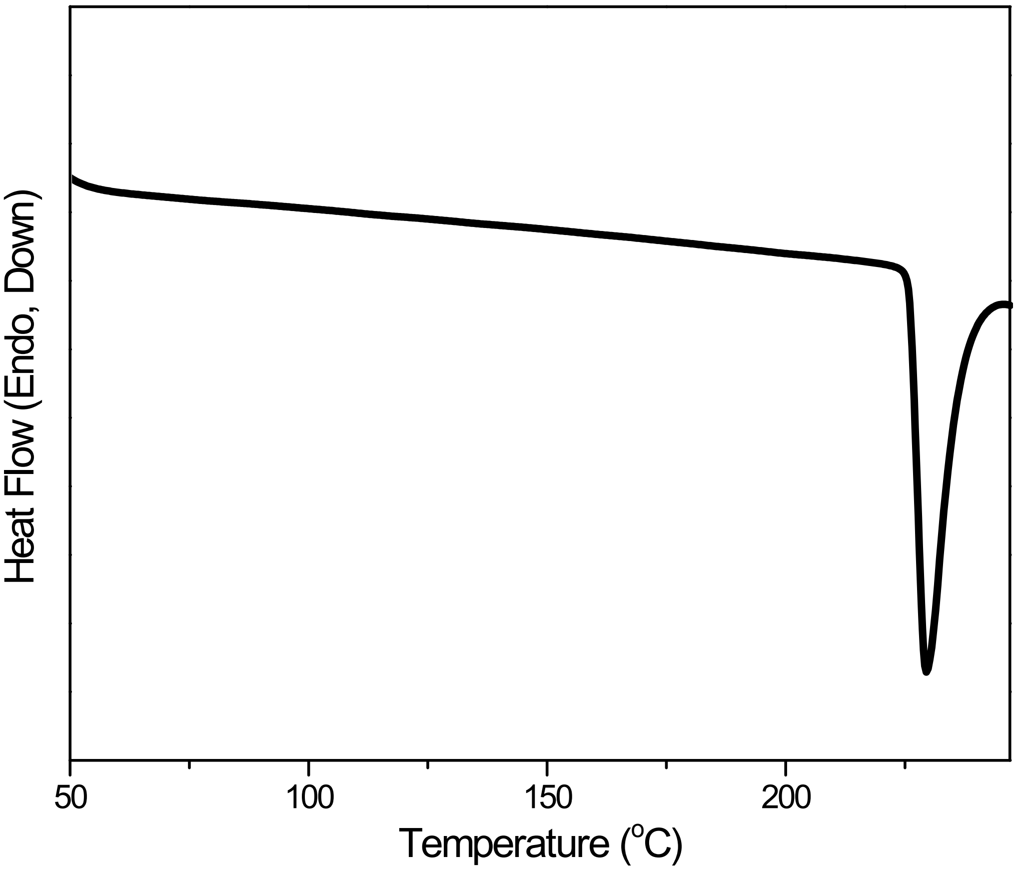

Figure S16. DSC profile of TPE.

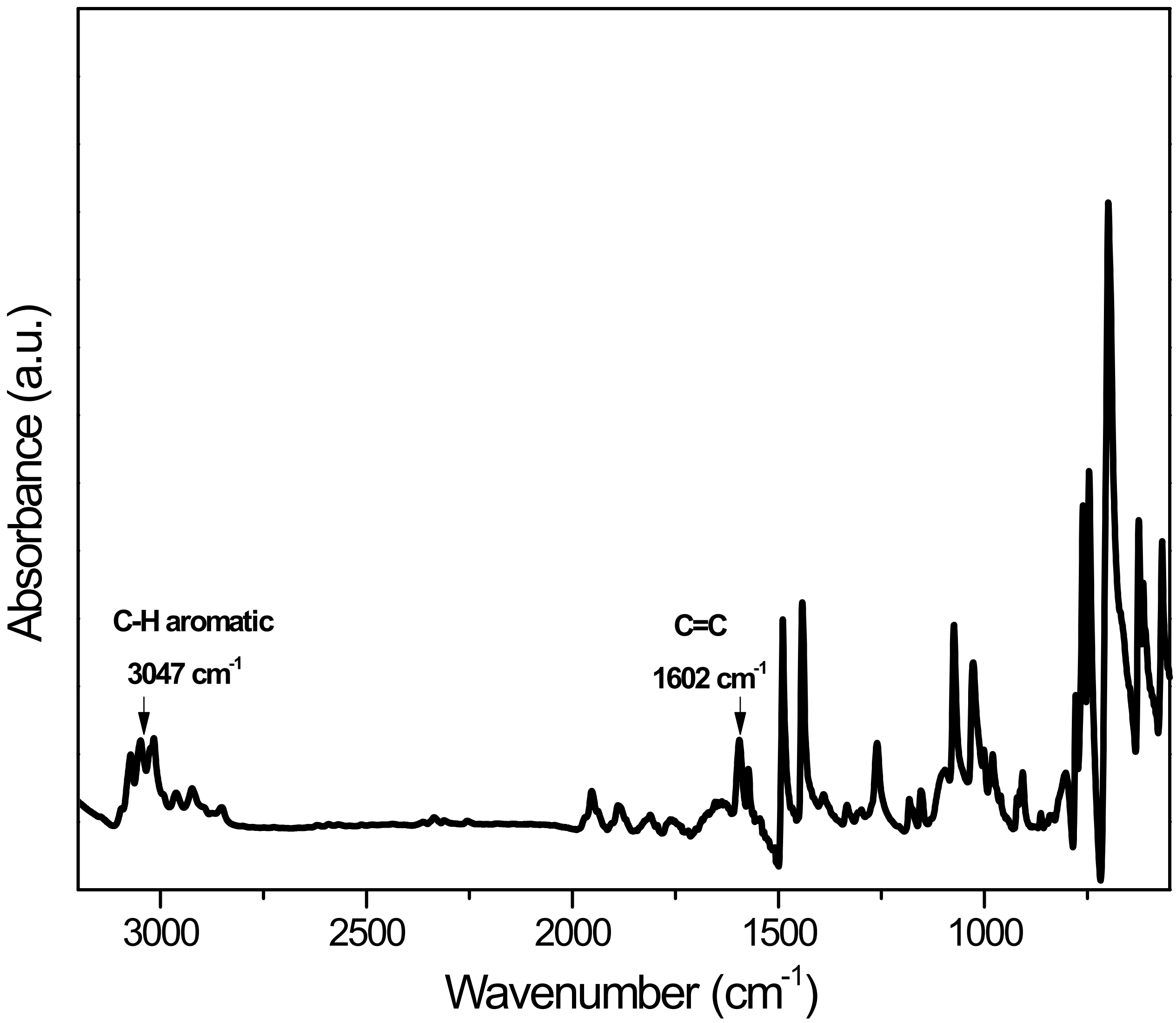

Figure S17. FT-IR spectrum of TPE.

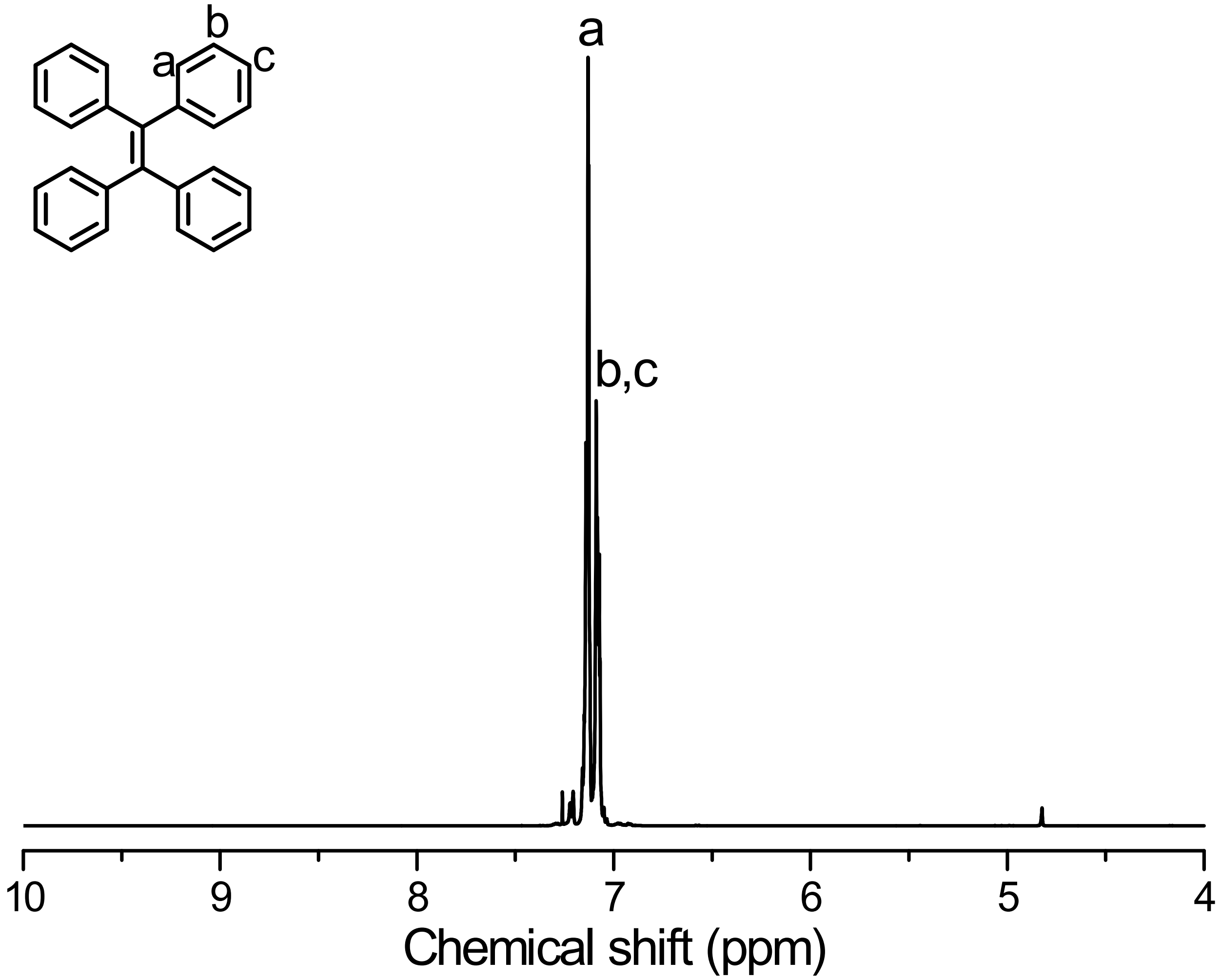

Figure S18. ^{1}H NMR spectrum of TPE.

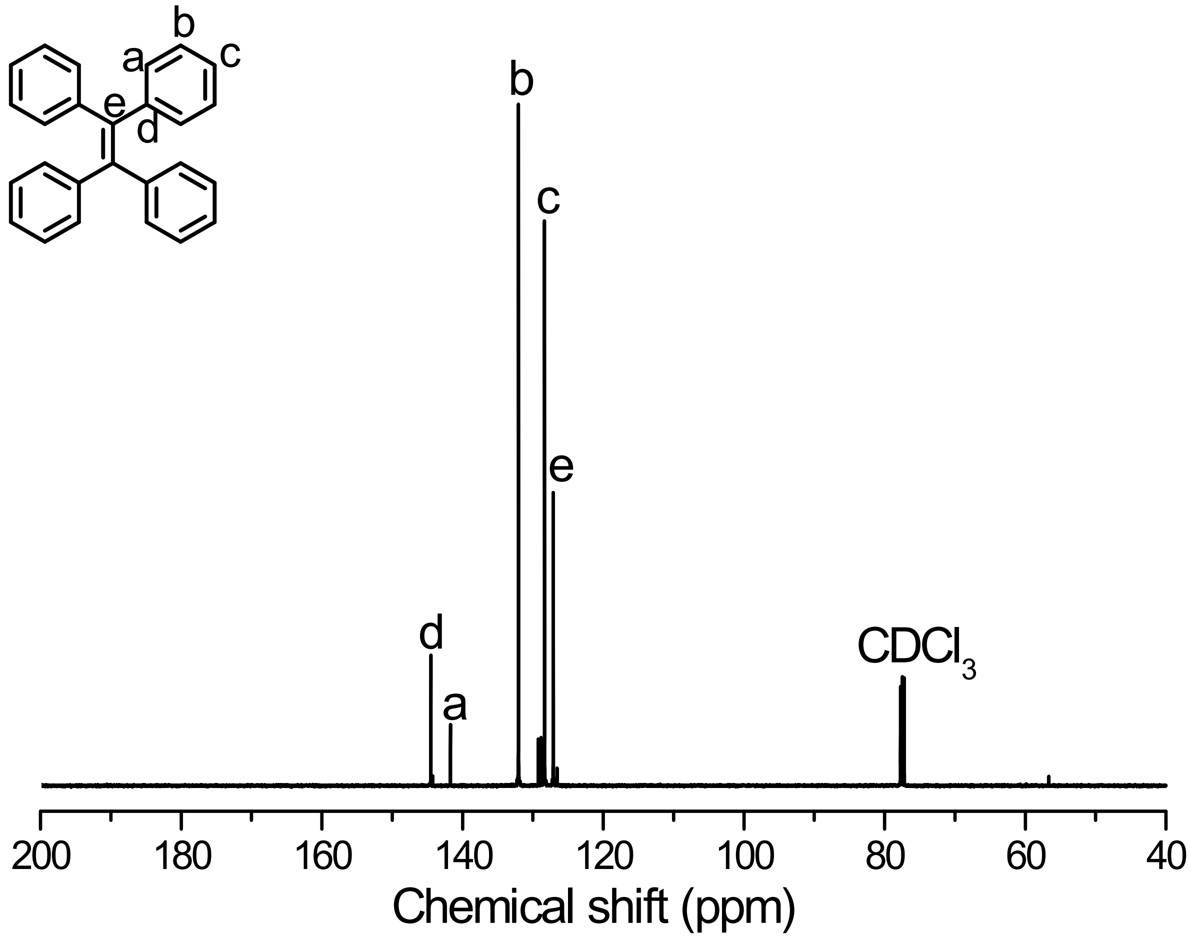

Figure S19. ^{13}C NMR spectrum of TPE.

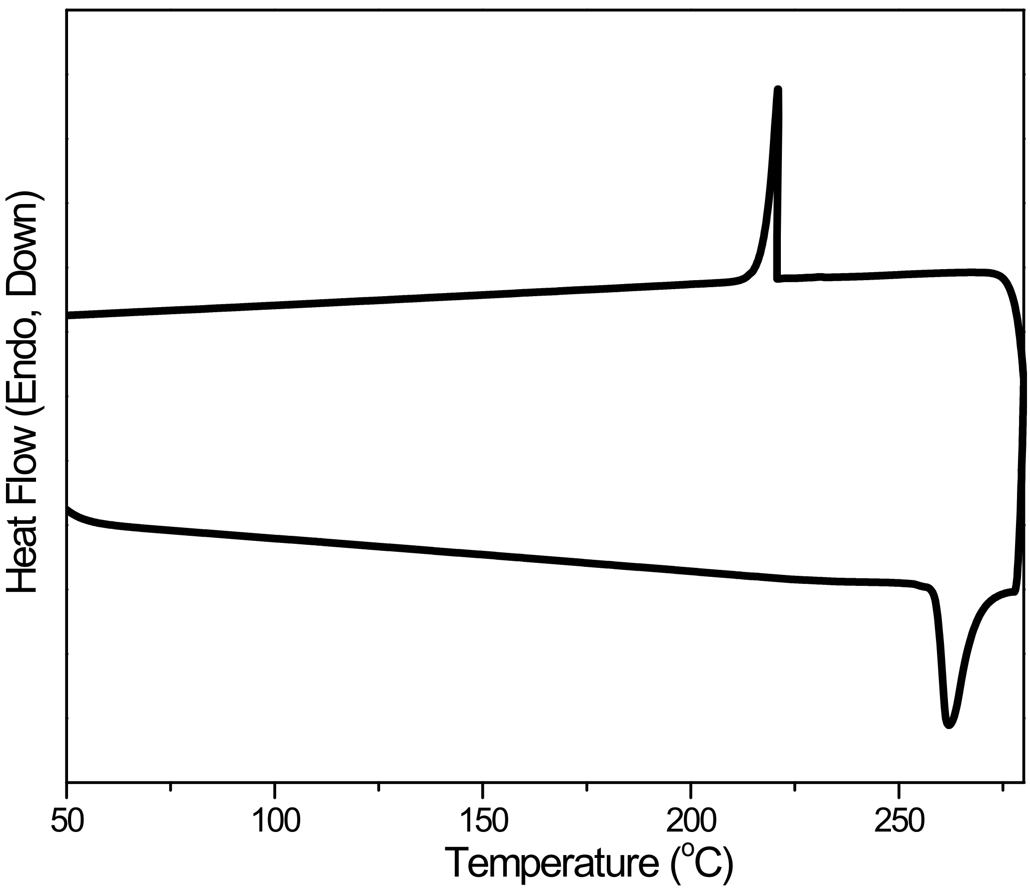

Figure S20. DSC profile of TPE-Br_4.

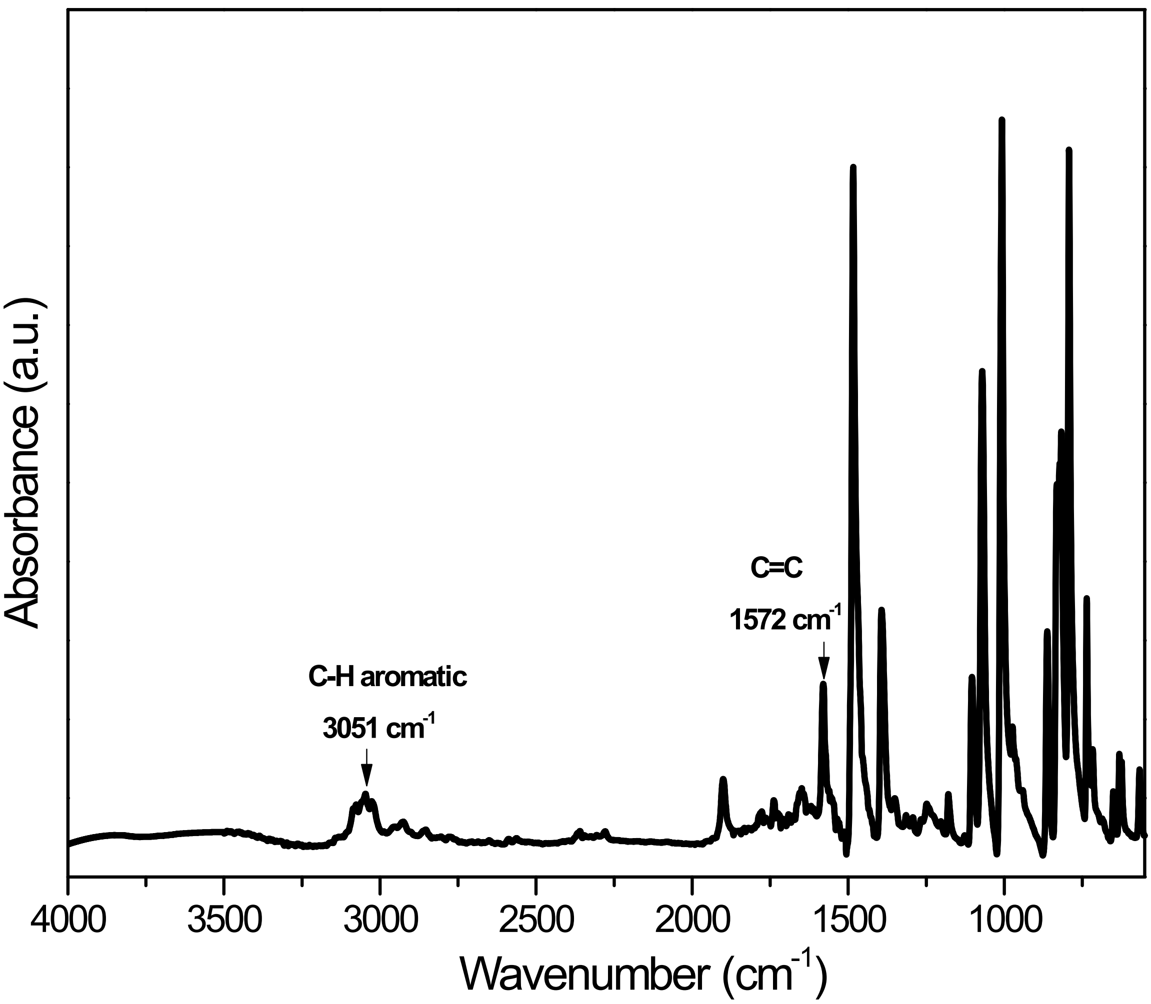

Figure S21. FT-IR spectrum of TPE-Br_4.

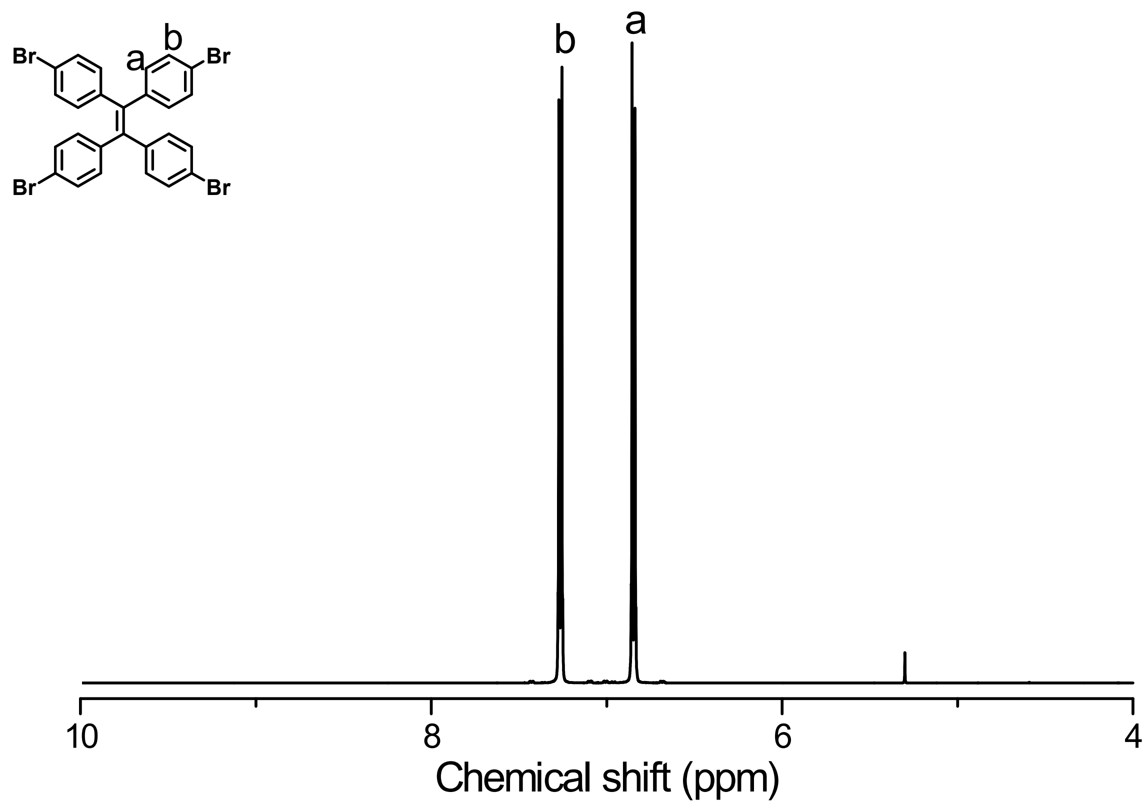

Figure S22. ^{1}H NMR spectrum of TPE-Br_4.

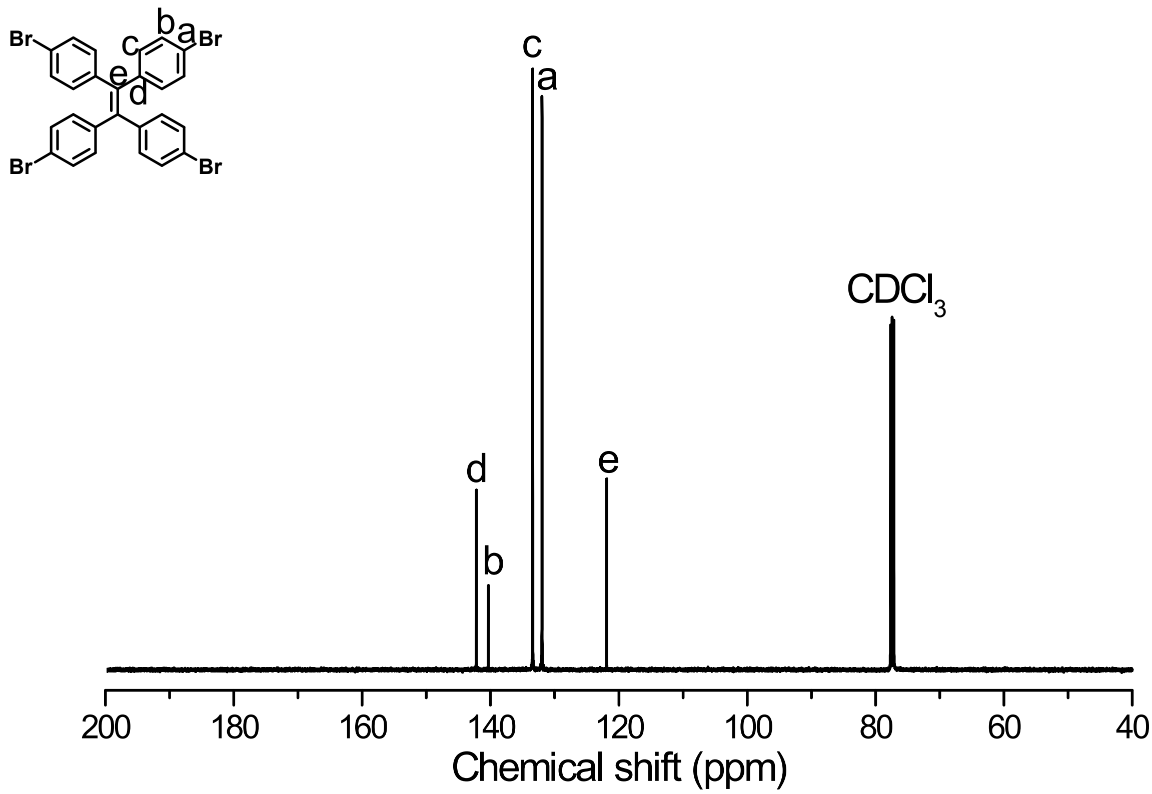

Figure S23. ^{13}C NMR spectrum of TPE-Br_4.

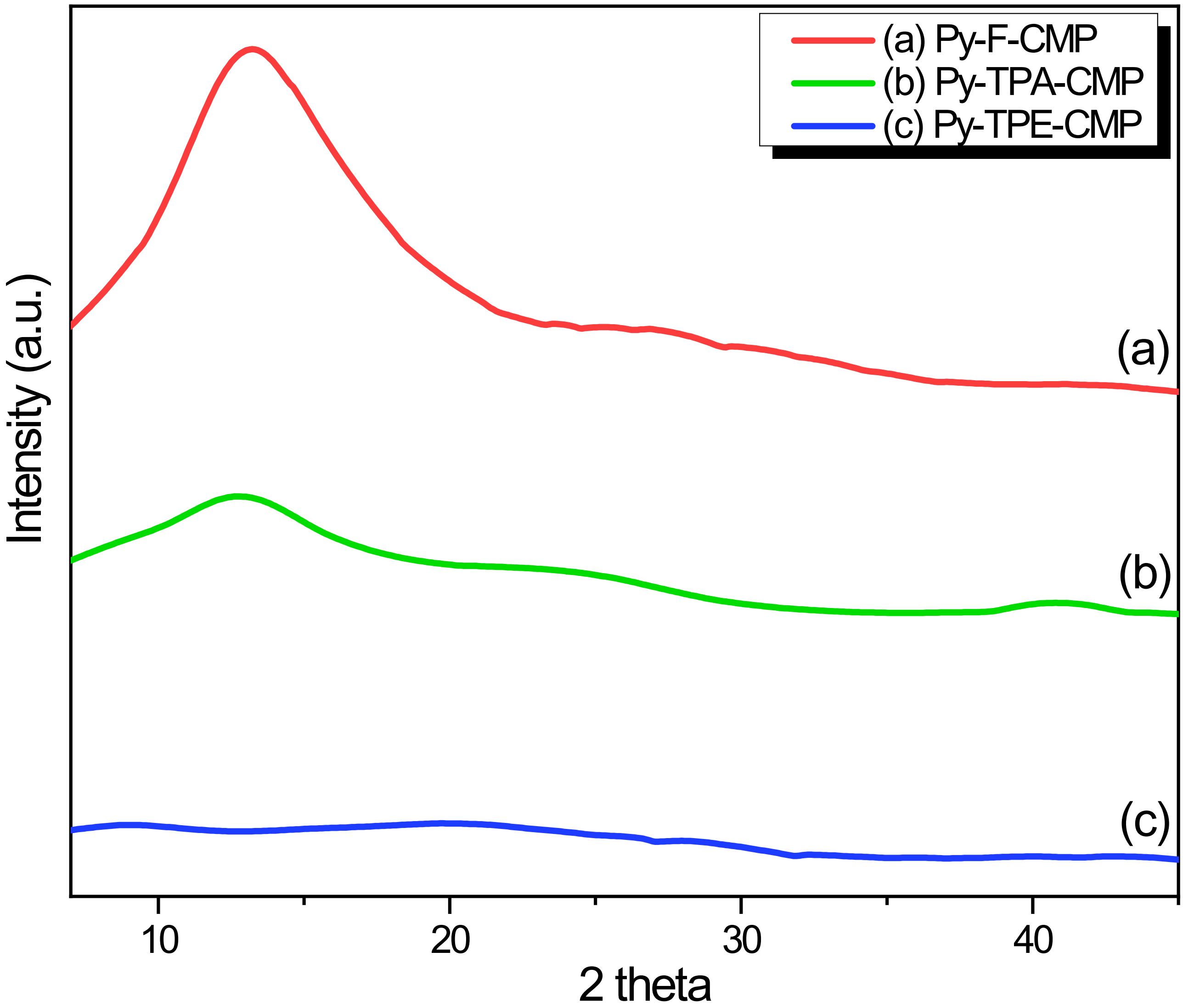

Figure S24. XRD profile of (a) Py-F-CMP, (b) Py-TPA-CMP and (c) Py-TPE-CMP.

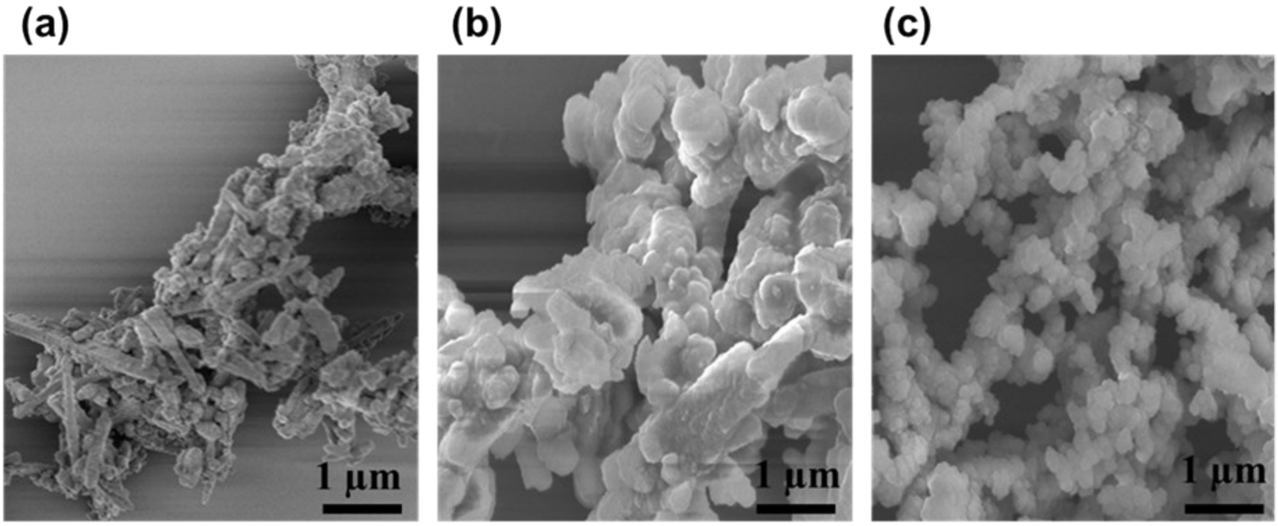

Figure 25. SEM images of (a) Py-F-CMP, (b) Py-TPA-CMP and (c) Py-TPE-CMP.

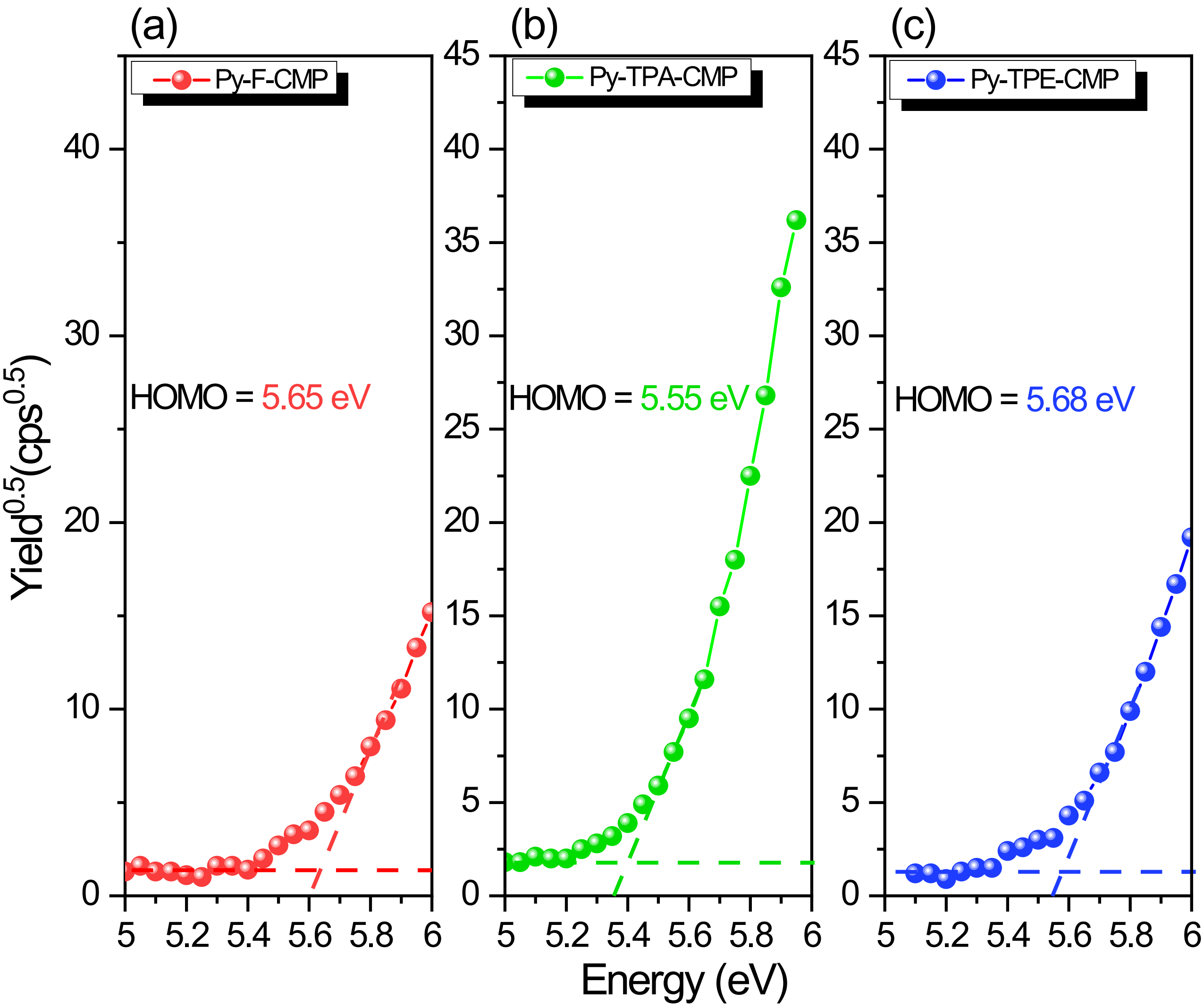

Figure S26. HOMO profiles of (a) Py-F-CMP, (b) Py-TPA-CMP and (c) Py-TPE-CMP.

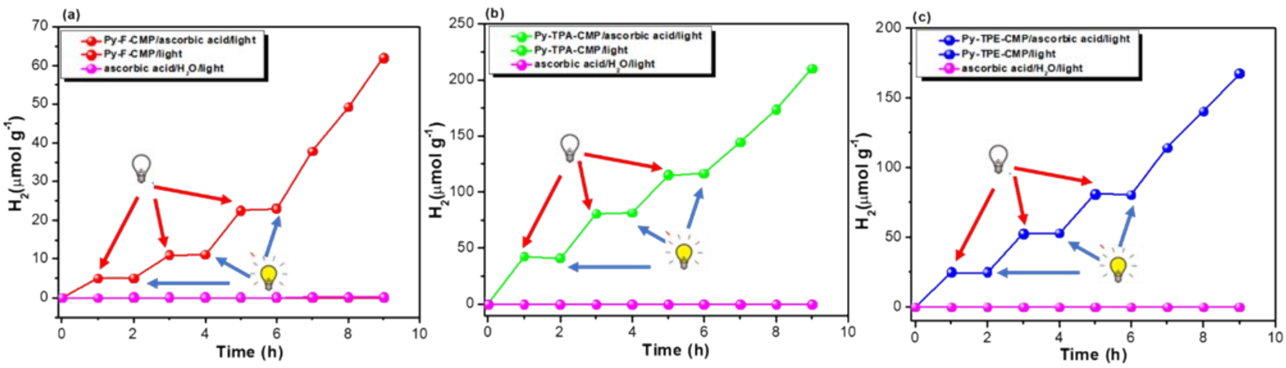

Figure S27. Control experiments for light-driven hydrogen generation from water at ambient temperature using (a) Py-F-CMP, (b) Py-TPA-CMP and (c) Py-TPE-CMP.

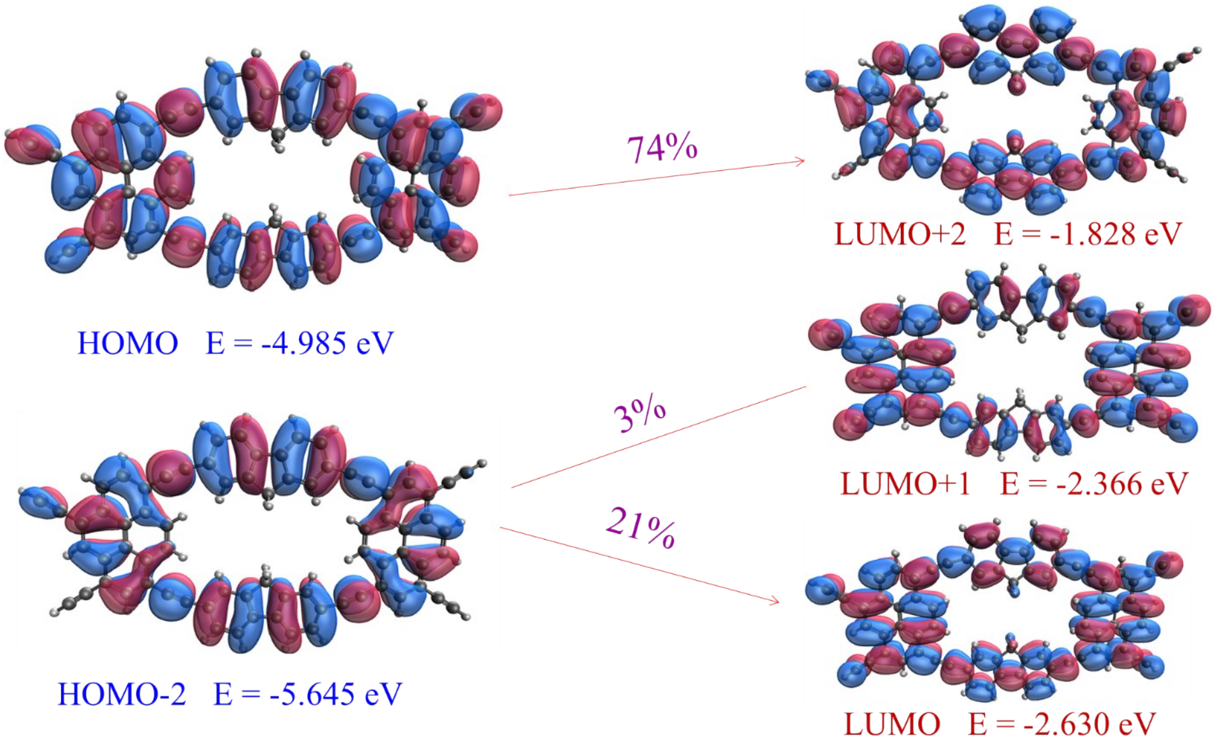

Figure S28. The excited states of the Py-F-CMP and the contribution of the transition between orbitals (the percentage on the arrow).

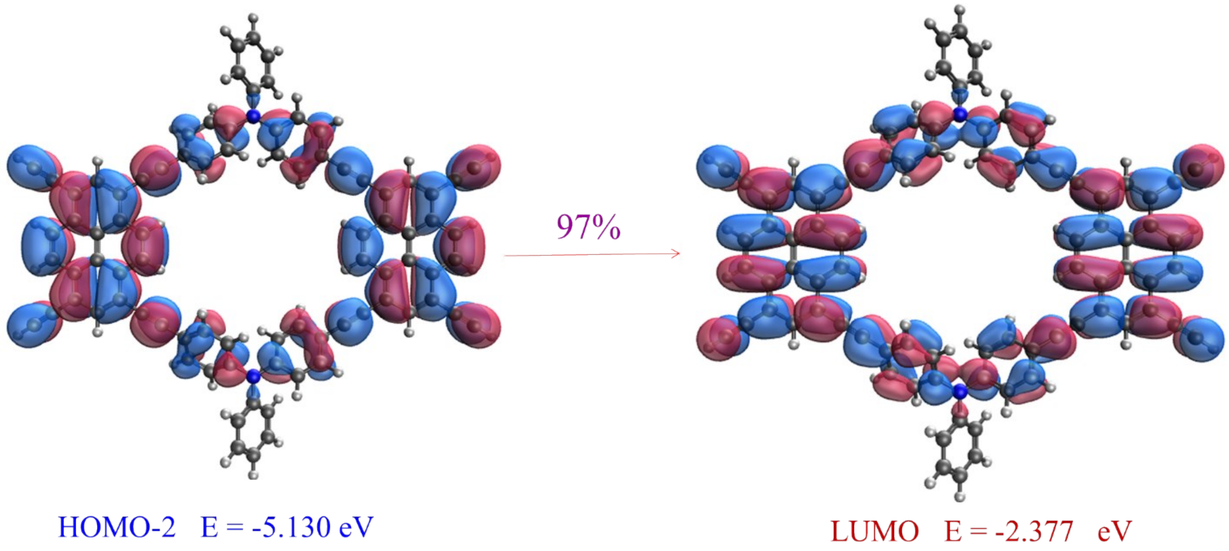

Figure S29. The excited states of the Py-TPA-CMP and the contribution of the transition between orbitals (the percentage on the arrow).

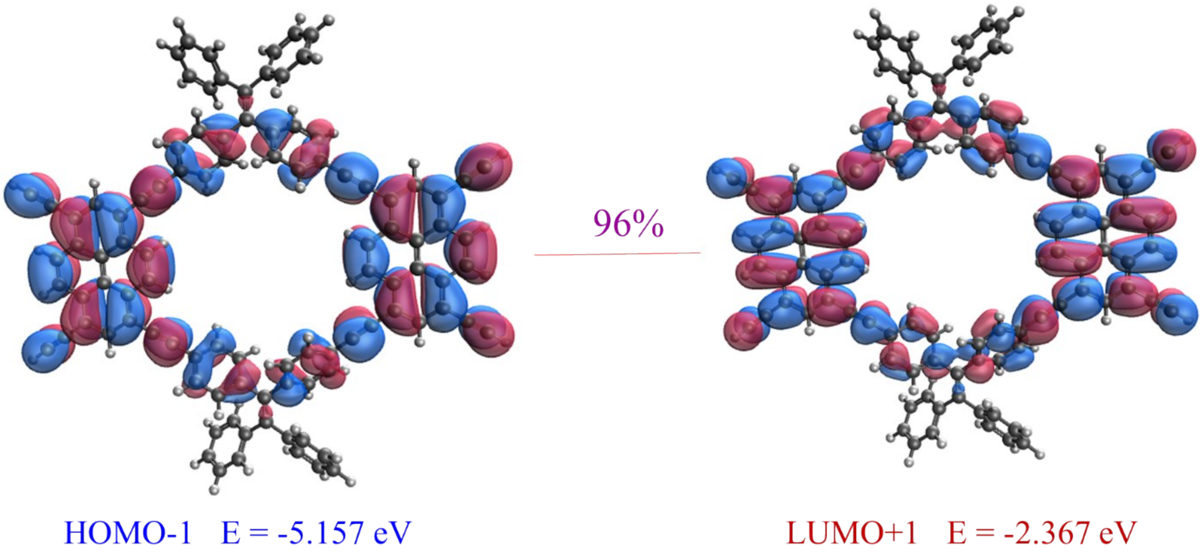

Figure S30. The excited states of the Py-TPE-CMP and the contribution of the transition between orbitals (the percentage on the arrow).

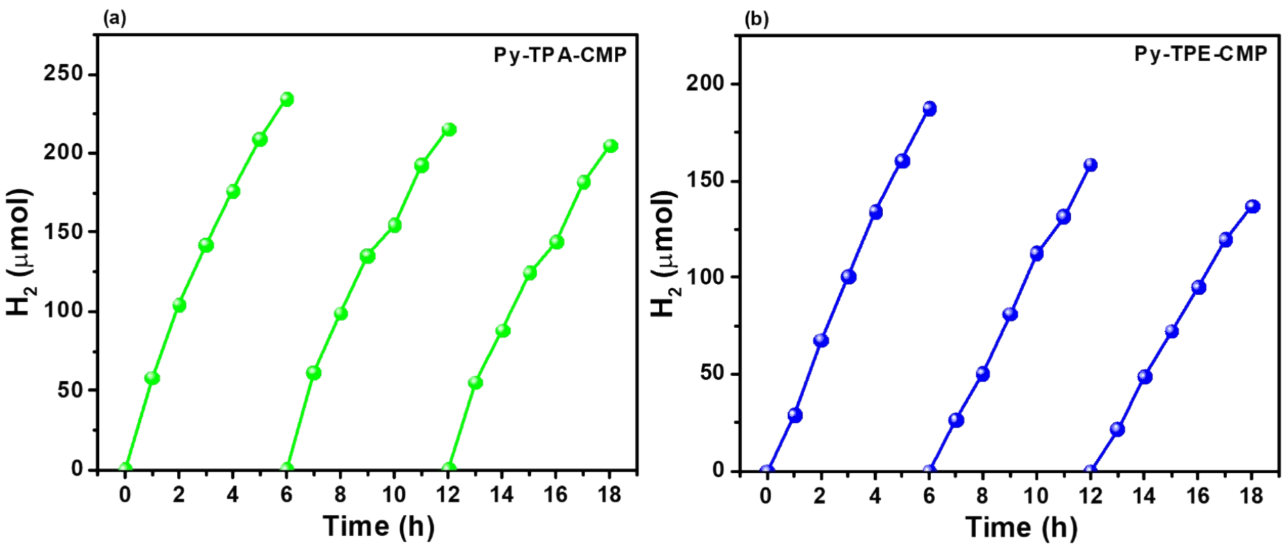

Figure S31. (a) and (b) Stability and recycling test using Py-TPA-CMP and Py-TPE-CMP as a photocatalyst under visible light irridation ($\lambda > 420$ nm).

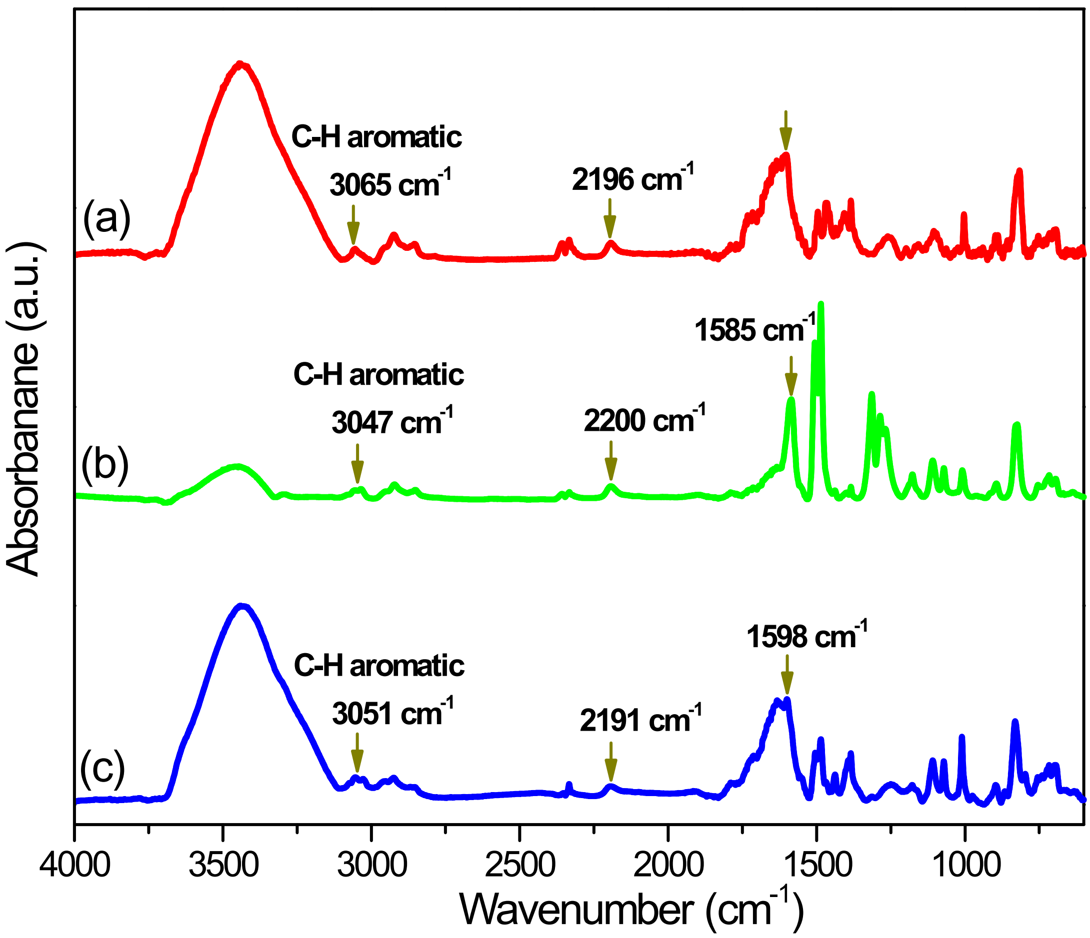

Figure S32. FTIR profiles of (a) Py-F-CMP, (b) Py-TPA-CMP and (c) Py-TPE-CMP after photocatalysts measurements.

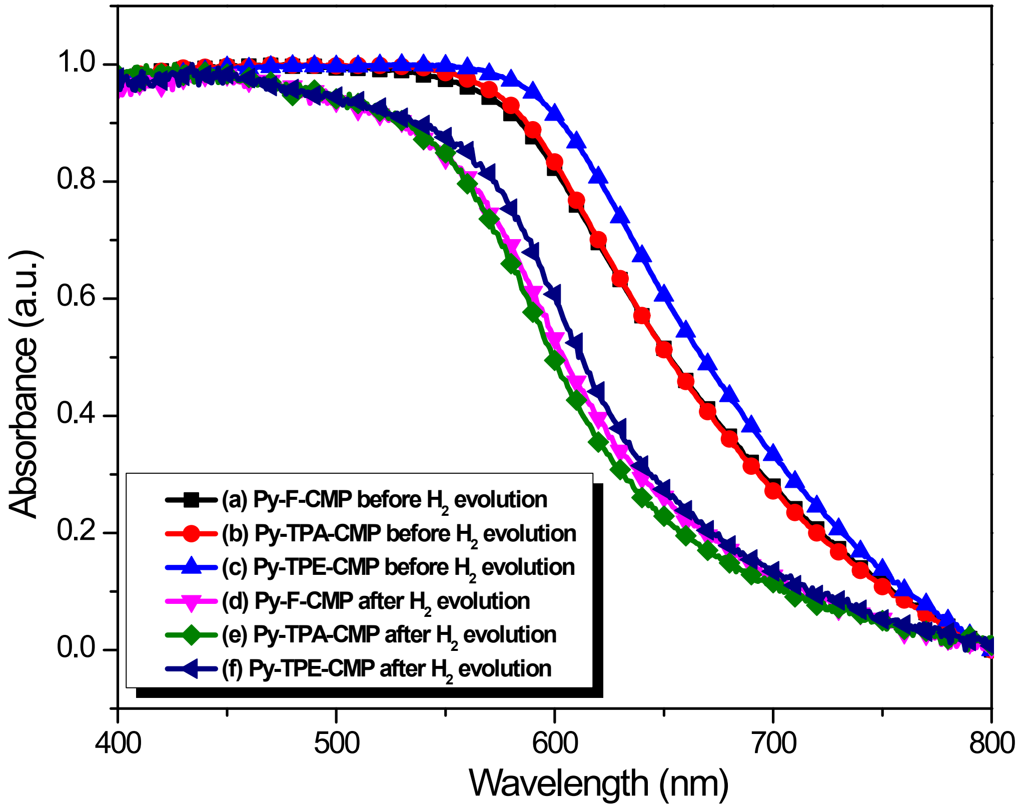

Figure S33. UV-Vis absorption spectra of (a) Py-F-CMP, (b) Py-TPA-CMP and (c) Py-TPE-CMP before photocatalysts measurements, and (d) Py-F-CMP, (e) Py-TPA-CMP and (f) Py-TPE-CMP after photocatalysts measurements.

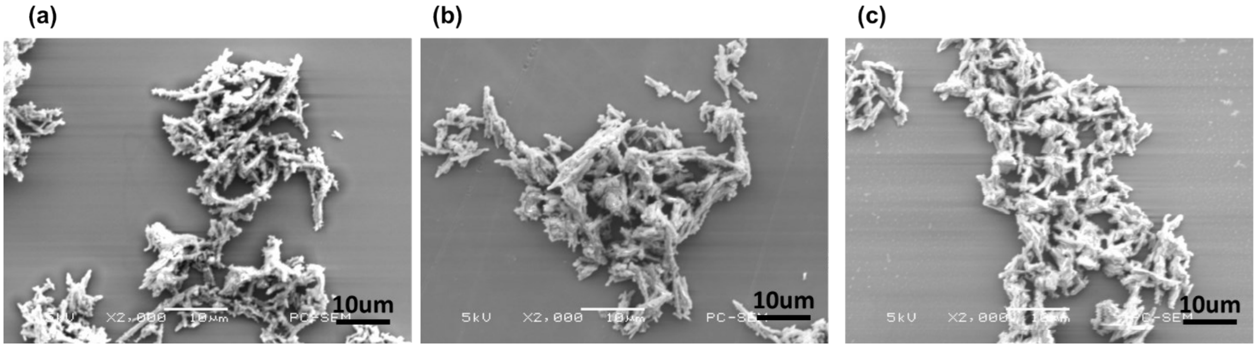

Figure 34. SEM images of (a) Py-F-CMP, (b) Py-TPA-CMP and (c) Py-TPE-CMP after photocatalysts measurements.

Table S1. Comparative studies of our designed pyrene-based microporous polymers with the reported CMPs in terms of photocatalytic hydrogen evolution.

Polymer Catalysts	**HER** $\lambda > 420$ nm **(μmol h^{-1})**	**HER** $\lambda > 420$ nm **(μmol h^{-1}g^{-1})**	**AQY %** λ > 420 nm	**Conditions**	**References**
COP-TP$_{0:1}$ COP-TP$_{3:1}$	9 42	900 4200	---- 1.5	Water/TEOA / 3 wt% Pt	**S1**
L-PyBT P-PyDFBT P-PyBT P-PyDFBT	83.7 20.9 0.3 1.5	1674 418 6 30	----	Water/TEOA / 3 wt% Pt	**S2**
P1	50	----	3.85	Water/TEOA / 3 wt% Pt	**S3**
Ta-CMP Ta-CMP-N Ta-CMP-CN	9.74 1.98 13.96	487 99 698	0.12 0.07 0.15	Water/TEOA	**S4**
4-CzPN	----	2103.2	6.4	Water/TEOA / 3 wt% Pt	**S5**
CP1 CP2 CP3 CP4	95.85 1.25 0.47 1.03	15975 208 78 172	---- ---- ---- ----	Water/AA /DMF	**S6**
TFPT-CH$_3$ TFPT-PDAN TFPT-OCH$_3$	4.4 11.8 22.1	---- ---- ----	--- --- 1.03	Water/TEOA / 3 wt% Pt	**S7**
S-CMP3	----	3,106	13.2	Water/ MeOH/TEO A	**S8**
P1 P2 P3 P4	50 0.9 22 1.3	1000 18 440 26	---- ---- 1.4 ----	Water/TEOA / 3 wt% Pt	**S9**
PyDF PyDM	--- ---	13470 1,280	4.5 -	Water/TEOA / 3 wt% Pt	**S10**
Py-TPA-CMP Py-TPE-CMP Py-F-CMP	57.5 39.1 16.8	19200 13033 5600	15.3 6.3 2.3	Water/ MeOH/AA/ 3 wt% Pt	This work

References

[S1] S. Nandy, T. Hisatomi, S. Sun, M. Katayama, T. Minegishi, and K. Domen, Effects of Se Incorporation in $La_5Ti_2CuS_5O_7$ by Annealing on Physical Properties and Photocatalytic H_2 Evolution Activity, *ACS Appl. Mater. Interfaces* 2018, **10**, 30698-30705.

[S2] C. Cheng, X. Wang, Y. Lin, L. He, J. X. Jiang, Y. Xu and F. Wang, The effect of molecular structure and fluorination on the properties of pyrene-benzothiadiazole-based conjugated polymers for visible-light-driven, *Polym. Chem*., 2018, **9**, 4468-4475.

[S3] J. Yu, X. Sun, X. Xu, C. Zhang and X. He, Donor-Acceptor Type Triazine-based Conjugated Porous Polymer for Visible-Light-Driven Photocatalytic Hydrogen Evolution, *Appl. Catal. B Environ*. 2019, **257***,* 117935.

[S4] K. Ding, Q. Zhang, Q. Li and S. Ren, Terminal Group Effect of Conjugated Microporous Polymers for Photocatalytic Water-Splitting Hydrogen Evolution, *Macromol. Chem. Phys*. 2019, **220**, 1900304.

[S5] G. Zhang, W. Ou, J. Wang, Y. Xu, D. Xu, T. Sun, S. Xiao, M. Wang, H. Li, W. Chen and C. Su, Stable, carrier separation tailorable conjugated microporous polymers as a platform for highly efficient photocatalytic H_2 evolution, Evolution, *Appl. Catal. B Environ*. 2019, **245**, 114-121.

[S6] W. Y. Huang, Z. Q. Shen, J. Z. Cheng, L. L. Liu, K. Yang, X. Chen, H. R. Wen and S. Y. Liu, C–H activation derived CPPs for photocatalytic hydrogen production excellently accelerated by a DMF cosolvent, *J. Mater. Chem. A*, 2019, **7**, 24222-24230.

[S7] K. Yu, S. Bi, W. Ming, W. Wei, Y. Zhang, J. Xu, P. Qiang, F. Qiu, D. Wu and F. Zhang, Sidechain-tuned π-extended porous polymers for visible light-activated hydrogen evolution, *Polym. Chem.*, 2019, **10**, 3758-3763.

[S8] R. S. Sprick, Y. Bai, A. A. Y. Guilbert, M. Zbiri, C. M. Aitchison, L. Wilbraham, Y. Yan, D. J. Woods, M. A. Zwijnenburg, and A. I. Cooper, Photocatalytic Hydrogen Evolution from Water Using Fluorene and Dibenzothiophene Sulfone-Conjugated Microporous and Linear Polymers, *Chem. Mater*. 2019, **31**, 305-313.

[S9] J. Yu, S. Chang, X. Xu, X. He, and C. Zhang, The effect of single atom substitution (O, S or Se) on photocatalytic hydrogen evolution for triazine-based conjugated porous polymers, *J. Mater. Chem. C*, 2020, **8**, 8887-8895.

[S10] X. Gao, C. Shu, C. Zhang, W. Ma, S. B. Ren, F. Wang, Y. Chen, J. H. Zeng and J. X. Jiang, Substituent effect of conjugated microporous polymers on the photocatalytic hydrogen evolution activity, *J. Mater. Chem. A*, 2020, **8**, 2404-2411.